# Simulation Experiments on the Spreading Behaviour of Core Melts: KATS-7

## (1-dim spreading of highly super-heated iron and oxidic melts into a dry channel at low pouring rates)

G. Fieg, F. Huber, H. Werle

Institut für Neutronenphysik und Reaktortechnik
Institut für Reaktorsicherheit
Projekt Nukleare Sicherheitsforschung

# Forschungszentrum Karlsruhe
## Technik und Umwelt

## Wissenschaftliche Berichte

## FZKA 6005

# Simulation Experiments on the Spreading Behaviour of Core Melts: KATS-7
# (1-dim spreading of highly superheated iron and oxidic melts into a dry channel at low pouring rates)

G. Fieg, F. Huber, H. Werle

Institut für Neutronenphysik und Reaktortechnik
Institut für Reaktorsicherheit
Projekt Nukleare Sicherheitsforschung

# ABSTRACT

In future Light Water Reactors special devices (core catchers) might be required to prevent containment failure by basement erosion after reactor pressure vessel meltthrough during a core meltdown accident. Quick freezing of the molten core masses is desirable to reduce release of radioactivity. Several concepts of core catcher devices have been proposed based on the spreading of corium melt onto flat surfaces with subsequent water cooling.

Therefore a series of experiments to investigate high temperature melt spreading on flat surfaces has been carried out using alumina-iron thermite melts as a simulant. The oxidic and metallic phases of the melt are separated and spread on different surfaces. The influence of a shallow water layer on the surface onto the spreading behaviour has also been studied previously.

In KATS-7 the spreading of an oxidic and metallic melt at high superheat temperatures into one-dimensional dry channels at low pouring rates has been investigated. The pouring rate of a corium melt from the reactor pit under the pressure vessel through a passively opened gate into the spreading area is a dominant factor for the spreading behaviour of the melt. KATS-7 was the first test within this KATS-series with a low pouring rate (about an order of magnitude below those of the preceeding tests).

The results show that in spite of much smaller spreading velocities (due to the low pouring rates), the spreading lengths for both melts are comparable to those of former experiments.

## Simulationsexperimente zum Ausbreitungsverhalten von Kernschmelzen: KATS-7

# ZUSAMMENFASSUNG

Für zukünftige Leichtwasserreaktor-Kraftwerke werden spezielle Einbauten (Kernfänger) erforderlich sein, um das Containment-Versagen infolge von Erosion des Fundamentes bei einem Kernschmelzunfall zu verhindern. Die geschmolzenen Kernmassen sollen möglichst schnell in einen festen Zustand übergeführt werden, um die Freisetzung von radioaktivem Material zu reduzieren. Einige der vorgeschlagenen Kernfängerkonzepte beruhen auf dem Prinzip, die geschmolzenen Kernmassen auf ebenen Flächen zu verteilen und anschließend mit Wasser zu kühlen.

Es wurde deshalb eine Serie von Experimenten durchgeführt, um das Ausbreiten von Schmelzen mit hoher Temperatur auf ebenen Flächen zu untersuchen. Dabei wurde als Simulationsmaterial eine Thermitschmelze aus Aluminiumoxid und Eisen verwendet. Die oxidischen und metallischen Komponenten werden getrennt und auf verschiedene Ausbreitungsflächen geleitet. Der Einfluß niedriger Wasserschichten auf den Flächen auf den Ausbreitungsprozeß wurde ebenfalls in früheren Experimenten untersucht.

In KATS-7 wurde die Ausbreitung einer oxidischen und metallischen Schmelze bei hoher Überhitzung und niedrigen Einströmraten in eindimensionale trockene Kanäle untersucht. Die Einströmrate einer Kernschmelze aus der Kaverne unter dem Druckbehälter durch ein sich passiv öffnendes Fenster in den Ausbreitungsraum des Kernfängers ist ein dominierender Faktor für das Ausbreiten der Schmelze. KATS-7 war der erste Test (innerhalb einer Serie von Experimenten), bei welchem im Vergleich zu früheren Tests die Einströmraten gering gehalten wurden. Sie lagen etwa eine Größenordnung unterhalb der früheren Werte.

Die Ergebnisse dieses Tests zeigen, daß trotz der deutlich niedrigeren Einströmraten die Ausbreitungslängen vergleichbar mit denen bei früheren Tests sind.

CONTENTS                                                   Page

# 1. INTRODUCTION

Special devices (core catchers) might be required in future Light Water Reactors to prevent containment failure by basement erosion after reactor pressure vessel meltthrough during a core meltdown accident. It is desirable to cool, preferably freeze, the molten core masses quickly in order to reduce the release of radioactivity and the danger of interaction of the melt with structural materials. This implies that thin layers of corium are formed on these structures. Several concepts of core catchers have been proposed to meet these requirements [1-4].
Also the core catcher foreseen for the European Pressurized Reactor (EPR) is based on these principles [5,6], fig.1. The basic concept of this device is to retain the corium masses in the cavern under the reactor pressure vessel long enough to collect most of the corium inventory after the breach of the pressure vessel. Afterwards a gate opens between the cavern and a spreading compartment, into which the corium melt is released. This gate opens as a result of erosion by the melt and the time period for this process has to be about one hour, which is long enough to gather most of the corium after the breach of the pressure vessel. This time period will also allow an increase of the melt temperature and correspondingly a decrease of viscosity to assure a fast spreading of the melt. The composition of the corium is 180 tons of oxidic melt ($UO_2$ and $ZrO_2$) and 120 tons of metallic melt (steel and Zr). Cooling of the melt is foreseen from the top by flooding the melt surface with water from top after the end of the spreading phase.

Corium melt spreading and subsequent interaction of spread corium with water during flooding are generic problems of the EPR core catcher and similar concepts. Models are under development to describe these phenomena. They have to be verified by experiments. The number of experiments with real molten corium will be limited; therefore, tests with appropriate simulant materials are required.

The spreading of corium onto concrete floors has been investigated theoretically [7,8]. In addition, Susuki et al. [8] conducted several spreading experiments using stainless steel melts to verify their modeling. Moody [9] modeled the spreading of corium melt onto a flat surface with and without overlying water. The MELTSPREAD-1 code [10] has been developed at the Argonne National Laboratory and describes the spreading of melts onto dry and wet surfaces. Malinovic et. al. [11] investigated spreading of thermite melts on dry and wet concrete surfaces and also studied the quenching rates due to overlying water pools. Greene et. al. [12] studied the spreading of a variety of materials onto wet and dry surfaces to derive correlations for spreading rates and lengths.

At Siemens/KWU the CORFLOW code [13] has been developed for EPR core catcher investigations. This code describes the spreading of melts onto dry surfaces and has been verified by low temperature melt spreading experiments at the CORINE facility [13]. In addition, CORFLOW

has to be verified with spreading experiments using higher temperature melts, and this is the main motivation for this series of experiments.

These tests are called KATS-experiments (abbreviation for Karlsruher Ausbreitungsexperimente mit Thermit-Schmelzen, Karlsruhe spreading experiments with thermite melts). Spreading experiments of separated alumina and iron melts on dry surfaces cannot directly simulate the spreading of real corium melts. The goal of these experiments is not to simulate as close as possible the behaviour of a corium melt, but to provide experimental data to validate CORFLOW. Therefore there is no need for a realistic scaling-up of the experimental layout to meet the EPR corecatcher design features. Knowledge of material properties, especially viscosity, for both, the simulant and the real melts is essential for extrapolating the results to reactor conditions using a computer model.

In this report the spreading of an iron and oxidic melt at high superheat into a dry one-dimensional channel at relatively low pouring rates is discussed.


## 2. EXPERIMENTAL SETUP

### 2.1 Test facility and thermite reaction

. The test rig, fig.2 shows schematically the principal setup, consists of a large reaction crucible for thermite to generate molten alumina and iron, two containers under the crucible to gather the separated melts and the spreading areas (channels). To avoid thermal attack the crucible wall consists of a ceramic material (mainly magnesia). Fig.3 shows a photo of the KATS facility. The thermite powder (300 kg) in the crucible is heated up to about 150 $^0$C for about 24 hours before ignition to release any moisture. Thermocouples inside the thermite powder and the crucible wall control this heating-up phase. At the bottom of the crucible a nozzle, 40 mm in diameter, is installed to discharge the melt. In contrary to former KATS-tests, which were provided with an pneumatically operated opening of the nozzle, in this test the melt release has been performed passively: in the lower part of the crucible, right above the nozzle, a slowly reacting thermite powder was loaded to a height of 100 mm, fig. 4. The reaction velocity of this special thermite is about 10 mm/s compared to 30 mm/s for the 300 kg load. With this method a delay time before melt release of approximately 10 s can be accomplished. This time is necessary to reach full separation of the metallic and oxidic phases. A 0.5 mm stainless steel metal foil closes the nozzle inlet to the crucible volume. Three thermocouples (type K) inside the slowly reacting thermite at different vertical positions detect the melt progress. Below the orifice two additional thermocouples of the same type have been installed to detect the melt

2

release. The output of these two thermocouples is connected to the control system to synchronize all further commands.

The thermite powder is ignited electrically at the top center of the load. The reaction time for a 300 kg load is about 25 s. Practical immediately during the thermite reaction the two phases of the melt, oxide and metal, separate in the crucible and the heavier iron melt is the first one which flows out of the nozzle. The iron melt container is positioned under the nozzle outlet. Under the chosen experimental conditions the pouring takes about 8 s for the iron melt. Once the metallic melt is exhausted, the jet is guided into the second container by a movable chute. In all preceeding tests (KATS-3b,-4,-5, and-6, [14,15,16]) the metallic and oxidic melts have been gathered in the two separate containers before spreading into the channels was initiated (by opening of gates in the containers). These containers are insulated with cordierite plates (52% $SiO_2$, 37% $Al_2O_3$, 6.5% MgO) with an open porosity of 23%. This material is highly resistant to temperature shocks and erosion due to high temperature melt jets. Some wall material of both containers is dissolved into the melts because of the low melt temperature of cordierite (1600 $^0$C). Due to incomplete chemical reaction and wall erosion the the oxidic melt is composed of about 85 weight% $Al_2O_3$, 5-10 weight% $SiO_2$ and about 5 weight% FeO. Estimated material properties of both melts are given Appendix A.

Different from the previous tests, in KATS-7 the two melts have not been gathered prior to the opening of the gate. The gates to the spreading surfaces were open from the very beginning. In this way low pouring rates, determined by the nozzle diameter, are achieved. To ensure an even spreading across the channel width, dams have been installed into both channels near the gate, figs. 5 and 6. These figures show the dimensions of the containers, gates, dams and spreading channels for the two melts. The according dimensions are listed in table 1 and define the main parameters at the onset of spreading. The melt overflows the dam after filling up the container to the dam's height. The pouring rate of the melt into the channel is controlled by the flow rate of the jet through the orifice. The quality of separation of the two melt phases depends strongly on the time, when the jet is guided from the iron container into the oxide container via the movable chute. For a certain time interval a mixture of oxidic and metallic melt flows through the nozzle. Therefore a complete separation was not possible with this method. In the case that the jet is directed too late into the oxidic container some oxidic melt is gathered in the iron container. The spreading of iron is not disturbed by this small amount of oxide above the iron melt. Yet, in the case that the jet is directed too early into the oxide container, some iron gathers at the bottom of the oxide container and spreads onto the surface together with the oxide melt. To minimize this risk, a "swamp" volume of more than 7 liters (equivalent to more than 40 kg of iron) has been provided for this excess iron melt in the oxide container.

3

The spreading channels are constructed of concrete covered with cordierite plates. The channels have been adjusted carefully with a slope of less than 1 mm over a length of 1 m against the horizontal. The iron channel was 230 mm wide and 11.5 m long, the oxide channel was 410 mm wide and 8.5 m long.

## 2.2 Instrumentation and Data Recording

During the spreading process the temperatures of both melts were measured with W-Re thermocouples at three different axial positions in the channel (0.3m, 1.8m and 4.8m), with the thermocouple junction level 10 mm above the channel floor. Thermocouples of type K (1 mm outer diameter) are positioned at different vertical positions (5, 15, 25 and 35 mm above the floor level) at different positions in the channel. These thermocouples have been installed to indicate the arrival time of the melt. Fig. 7 and table 2 show the positions and identification of the different measuring points. In addition to these thermocouples several video-cameras recorded the spreading process.
The measured and amplified thermocouple signals were recorded using a digital 32 channel transient recording system. A sampling rate of 1kHz per channel was applied leading to an overall recording time of 256 s. The transient recorder was started with the release of the melt from the reaction crucible. The trigger signal is from signals of the two thermocouples which are positioned under the crucible orifice. After conduct of the experiment the recorded data were transferred and stored on a disk. The evaluation is done with a special computer program supplied together with the transient recording system. For synchronisation reasons of the different video recorders flashlights were triggered together with the commands for thermite ignition and opening of the gates.

## 2.3 Control System

The commands during conduct of the tests (thermite ignition, moving the chute, start of the transient recorders and firing flashes for synchronization of the video cameras with the electronic data system) are controlled by an electronic control system. After ignition the system gets into a waiting queue to receive the signal from one of the two thermocouples under the orifice. The duration for the thermite reaction has been estimated with an established rule of thumb: the reaction front velocity proceeds at about 30 mm/s for the thermite powder as used in these tests. For the height of the thermite powder (0.8 m) this reaction time is about 26 s. The additional reaction time for the lower thermite load is necessary for outgassing and full separation of the two melt phases.

Table 3 shows the timing of the different commands during conduct of the experiment.

## 3. RESULTS

## 3.1 Pouring rates

Only 22.1 s after ignition of the thermite powder, much earlier than estimated, melt release happened. The reason for this early release may be a faster progress of the reaction front than has been calculated in advance. This early melt release was also the reason for the relative high melt temperatures. As mentioned in the preceeding chapter, the pouring rates of both melts are controlled by the flow through the nozzle located at the bottom of the reaction crucible. At the onset of the test the inner diameter of the orifice was 40.0 mm. Post experimental analysis showed that this diameter has increased up to 63 mm during melt flow. A total time of 25.5 seconds of melt flow was registered with the help of thermocouple readings and videorecording. After conduct of the test 124.5 kg of iron were found in the iron channel and 0.5 kg in the iron container. The rest was gathered in the oxide container (1 kg) and in the oxide channel (about 31.6 kg). 8.5 seconds after start of melt release the control system gave the command to move the chute. 2.0 seconds later the melt jet was guided into the oxide channnel. From these data the time dependancy of the pouring rates for both metallic and oxidic melts can be calculated. The form of the orifice has been chosen to produce a smooth jet. The discharge coefficient [17] of the orifice was varied between 0.7 and 0.9 for this analysis and it turned out that a coefficient of 0.8 fitted the experimental data best. Several calculations have been performed under different assumptions of the transient erosion behaviour of the nozzle: A linear and a square increase in diameter with time from the very beginning of melt release; a constant diameter until the iron melt is exhausted and then a linear respectively a square increase of the diameter. The square law of diameter increase from the very beginning meets the experimental data best, fig. 8. Erosion of the ceramic nozzle due to iron is small, oxidic melts have a larger erosion effect on oxidic materials. From these results volumetric flow rates for both, metallic and oxidic, melts can be derived. Table 4 show these recommended pouring rates. For both melts time zero is identical with the start of the spreading (melts start to overflow the dams). Those time intervals to fill up swamp volumes in the containers are not included in these tables.

5

## 3.2 Spreading of the iron melt

Immediately after melt release the relatively small volume behind the dam has been filled up and the spreading process started. Due to the existence of this dam the spreading was rather homogeneous across the 23 cm wide test section. In fig. 9 the leading edge of the iron melt across the channel width is shown for different spreading times. The data are from video recording. Only towards the end of spreading, close to the time of immobilization, the spreading front was not that even any more.

The transient W-Re thermocouple signals are shown in fig. 10. Close to the dam the melt temperature was 2295 $^0$C. This value is higher than those of similar preceeding experiment because of the early melt release from the crucible and the immediate spreading without gathering the melt in the container for a certain time. As to the preceeding tests, the melt has been gathered in the containers before spreading which caused some additional heat losses. Further downstream the temperature of the spreading iron melt was 2180 $^0$C (at 1.8 m) and 1950 $^0$C (at 4.8 m) which gives an average temperature drop of 70 K/m along the spreading channel.

Table 5 shows the arrival times of the iron melt at the location of the K-type thermocouples. Included in this table are also the average velocities which are calculated from these thermocouple readings. The corresponding transient thermocouple registrations are shown in figs. 11 - 13. The evaluation of arrival times from these registrations is not possible for all thermocouple locations in the channel, especially for longer spreading distances.

The maximum spreading velocity was 0.4 m/s at the beginning of spreading and decreased steadily with time. This maximum spreading velocity is similar to the input flow velocity of the iron melt entering the channel at the location of the dam. This velocity is calculated by dividing the input volume flow through the window size (which is 2 cm height by 14.5 cm width for the iron case). The transient spreading of the iron melt has also been analyzed with the video recordings, fig. 9, and is shown together with the thermocouple readings (at 5 mm vertical height) in fig. 14. At a distance of 7.8 m the iron melt stopped to spread further into the channel. At the time of immobilization the whole iron slag was still in a liquid state as can be detected by the video recordings. After cooling down to ambient temperature the iron slag shrinked by about 100 mm in axial direction.

Post experimental examination of the iron slag in the channel has been done. A total mass of 124.5 kg of iron spread into the channel. Some of the remaining iron is found inside the iron container (0.5 kg) and oxide container (1 kg). A larger amount (33.8 kg=5-6 liters) has been found in the oxide channel. A swamp volume of about 7 liters in the oxide container was foreseen to gather surplus iron. There is no explanation yet why the iron melt did not gather in this swamp volume. A possible one may be

6

found in the fact that the melt release from the reaction crucible happened too early and the thermite reaction was not yet fully finished. This unforeseen faulty behaviour was the reason why KATS-7 was the last test with this kind of melt separation, from the KATS-8 test on another, more successful, method has been applied.

The erosion of the cordierite material of the spreading surface was very minor. The average height of the solid iron slag was 8.9 mm, close to the value of 9.1 mm as found in test KATS-6. Due to different densities between liquid and solid iron a correction has to be done to get the average height of the liquid slag at the time of immobilisation, also the fact of shrinking had to be accounted for. So, at the time of immobilisation the average height was calculated to be 10.8 mm. The leading edge velocity of the melt and consequently its inertia force is very small towards the end of spreading. The viscosity of liquid iron does not change much with temperature. Immobilisation of the iron is therefore not due to increasing viscosity, but rather due to the surface tension of liquid iron. As for test KATS-6 with a simple analytical expression between the gravitational force of the slag and the surface tension at the front of the slag the melt height of can be calculated. When inertia forces can be neglected, which is the case towards the end of spreading, gravitation and surface tension are the dominating forces:

Gravitational pressure: $p_g = \rho \cdot g \cdot h$

Surface tension pressure: $p_s = \dfrac{2 \cdot \sigma}{r}$

h=melt height
r=h/2=curvature radius at the front
σ=1.45 N/m surface tension of iron at melt temperature
ρ=6300 kg/m³ specific density of liquid iron

The resulting melt height h at which the two pressures are balancing each other, is:

$h = \sqrt{\dfrac{4\sigma}{\rho g}} = 9.7mm$, which is in rather good agreement with the experimental value (10.8 mm).

## 3.3 Spreading of the oxide melt

10.5 s after melt release the jet has been guided into the oxide container due to the moving chute. A swamp area of 7 liters had first to be filled up before the spreading could start. Due to the dam construction, fig.6, the spreading was rather homogeneous across the channel width of 41 cm. The leading edge of the melt across the channel width is shown in fig. 15 for  different spreading times. The data are from video recording of the spreading melt. Fig. 15 shows that disturbances of the leading edge front by the thermocouples are damped further downstream.

The temperature recordings of the W-Re thermocouples at three axial positions (0.05 m, 1.8 m and 4.8 m, measured from the dam) are shown in fig. 16. The temperature at the channel entrance was 2200 $^0$C. Further downstream at 1.8 m and 4.8 m the temperature was appreciably lower, 2110 $^0$C resp. 1920 $^0$C. One has to take into account that the response time of these relatively large C-type thermocouples is about 4 seconds. At the time when the third thermocouple at 4.8 m reached its asymptotic value, the  melt already arrived its final spreading at 5.9 m. Table 6 shows the arrival times at the type K thermocouples locations. Included are also the average velocities as calculated from the thermocouple readings. Figs. 17-19 show the corresponding transient registrations for these thermocouples. As in the case of iron melt spreading, also here the evaluation of arrival times from these registrations is not possible for all thermocouple locations in the channel, especially for longer spreading distances.

The maximum spreading velocity is about 0.4 m/s at the beginning and decreases steadily with time. The transient spreading of the oxide melt can be analyzed with the videorecordings. Fig. 20 shows these results together with the K-type thermocouple recordings at 5 mm vertical positions. The final spreading length was 5.9 m. Immobilization of the oxide melt must be attributed to the rapidly increasing viscosity at lower temperatures. This result can be drawn by comparing the transient spreading and the corresponding temperature recordings of the melt.

Post experiment analysis revealed that the erosion of the cordierite material in the oxide channel was rather large: about half of the 20 mm thick plates has been eroded in the range from the dam to about 1 m in the channel. During the spreading process molten cordierite material mixed and spread with the oxide melt. The oxide layer thickness varies strongly with the channel position: from more than 70 mm near the entrance to about 20 mm towards the end of the oxide slag. Porosities between 25% and 35% are found. They are mainly due to outgassing of the bottom cordierite plates which have a porosity of 23%.

# 4. SUMMARY

The one-dimensional spreading of an iron and oxide melt at high superheat temperatures and low pouring rates into dry channels has been studied.The spreading distances of both melts were found to be only slightly less than those of similar previous experiments with pouring rates which were more than an order of magnitude higher. From this result the conclusion can be drawn that as long as melts are at high superheat temperatures their spreading distances are rather large and not much dependant of their pouring rates.

# 5. REFERENCES

1.  J.D. Fish, M. Pilch and F. Arrellano, "Demonstration of Passively-Cooled Particle-Bed Core Retention," Proceedings of the 5th Post Accident Debris Cooling Information Exchange Meeting, Karlsruhe, Germany,28-30 June 1982, 319-324

2. H. Alsmeyer et. al., "Improved Containment Concepts for Future Large LWR's," IEA Int. Conf. Technology Responses to Global Environmental Challenges, Kyoto, Japan, 6-8 November 1991, 471-489

3. A. Turricchia, "How to Avoid Molten Core/Concrete Interaction and Steam Explosions," Proc. 2nd Organization for Economic Cooperation and Development Committee on the Safety of Nuclear Installations Specialist's Meeting on Molten Core Debris-Concrete Interaction, Karlsruhe, Germany, April 1992, KfK-Report 5108, 503-518

4.  J.M. Seiler, F. Balard, M. Durin, A. Méjane, S. Pigny and I. Szabo, "Conceptual Studies of Core Catchers for Advanced LWR's," Proc. Int. Conf. Design and Safety of Advanced Nuclear Power Plants, Tokyo, Japan, October 25-29, 1992, Vol III, p. 300-327

5.  M. Michel et. Al., "EPR Safety Approach and Consideration of Severe Accidents,"Transactions of the ENC '94, Lyon, France, October 2-6,1994, Vol.II,502-506

6.  M. Fischer, Siemens/KWU, private communication, May 1996

7.  M.S. Kazimi,  "On the Liner Failure Potential in MARK-I Boiling Reactors," Nucl. Science and Engineering, **103**, 59-69 (1989)

8.  H. Suzuki, T. Mitadera, I. Sakaki and T. Zama, "Fundamental Experiment and Analysis for Melt Spreading on Concrete Floors," Proc.

Intern. Conference on Nucl. Energy (ICONE-2), San Francisco, March 21-24, 55-59,1993

9.  F.J. Moody, "First Order Analyses of Molten Corium Heat Transfer," ANS Proc. 1989 National Heat Transfer Conference, August 6-9, 1989, Philadelphia, PE, 217-224

10. M.T. Farmer, J.J. Sienicki, B.W. Spencer and C.C. Chen, "Status of the MELTSPREAD-1 Computer Code for the Analysis of Transient Spreading of Core Debris Melts," Proc. 2nd Organization for Economic Cooperation and Development Committee on the Safety of Nuclear Installations Specialist's Meeting on Molten Core Debris-Concrete Interaction, Karlsruhe, Germany, April 1992, KfK-Report 5108, 489-502

11.    B. Malinovic and R. E. Henry, "Experiments Relating to Drywell Shell-Core Debris Interaction", EPRI-NP 7196L (February 1991)

12. G.A. Greene, K.R. Perkins and S.A. Hodge,"Mark I Containment Drywell-Impact of Core/Concrete Interactions on Containment Integrity and Failure of the Drywell Liner," Proceedings of an International Symposium on Source Term Evaluation for Accident Conditions, Columbus,OH, October 28-November 1, 1985, pp 429, International Atomic Energy Agency, Vienna, (1986).

13.    J. M. Veteau and R. Wittmaack, "CORINE Experiments and Theoretical Modelling," FISA-95 Symposium - EU Research on Severe Accidents, Luxembourg, Nov. 20-22, 1995, 271-285

14. M. Steinbrück: EquiTherm-calculations, private communication

15. M. Steinbrück: GEMINI-calculations, private communication

16. G. Fieg, H. Werle, F. Huber, "Simulation experiments on the spreading behaviour of molten core melts:KATS-3b and KATS-4",Forschungszentrum Karlsruhe, Wissenschaftlicher Bericht FZKA 5887, 1997

17 G. Fieg, H. Werle, F. Huber, "Simulation experiments on the spreading behaviour of core melts:KATS-5 (1-dim spreading of an oxidic melt into a dry channel)", Forschungszentrum Karlsruhe, Wissenschaftlicher Bericht FZKA 5920, 1997

18. Dubbel Taschenbuch für den Maschinenbau, Springer Verlag,
    17. Auflage, 1990, B52-B53

# ACKNOWLEDGEMENTS

## Table 1   Dimensions of oxide and iron melt containers and spreading channels for the KATS-7 test

|  | Unit | Oxide | Iron |
|---|---|---|---|
| Container inner width | cm | 37.8 | 17.8 |
| Container inner depth | cm | 32.5 | 32.5 |
| Vertical opening near dam | cm | 2.0 | 2.0 |
| Release gate width | cm | 34.0 | 14.0 |
| Dam height | cm | 3.5 | 6.5 |
| Channel width | cm | 41.0 | 23.0 |
| Channel length | m | 8.5 | 11.5 |

[1]) Data derived from post experimental examination

11

# Table. 2  Location of thermocouples in test KATS-7

| Axial position of thermocouples (m) | Iron channel Thermocouple # Vertical positions of thermocouples | | | |
|---|---|---|---|---|
| | 5 mm | 15 mm | 25 mm | 35 mm |
| 0.05 | E.TW.0005 | - | - | - |
| 0.3 | E.TK.0305 | - | - | - |
| 1.8 | E.TK.1805 E.TW.1805 | E.TK.1815 | E.TK.1825 | E.TK.1835 |
| 3.3 | E.TK.3305 | - | E.TK.3325 | - |
| 4.8 | E.TK.4805 E.TW.4805 | E.TK.4815 | E.TK.4825 | - |
| 6.3 | E.TK.6305 | - | - | - |
| 7.8 | E.TK.7805 | - | - | - |
| 9.3 | E.TK.9305 | - | - | - |
| 10.8 | E.TK.10805 | - | - | - |

| Axial position of thermocouples (m) | Oxide channel Thermocouple # Vertical positions of thermocouples | | | |
|---|---|---|---|---|
| | 5 mm | 15 mm | 25 mm | 35 mm |
| 0.05 | O.TW.0005 | - | - | - |
| 0.3 | O.TK.0305 | - | - | - |
| 1.8 | O.TK.1805 O.TW.1805 | O.TK.1815 | O.TK.1825 | O.TK.1835 |
| 3.3 | O.TK.3305 | O.TK.3315 | O.TK.3325 | - |
| 4.8 | O.TK.4805 O.TW.4805 | O.TK.4815 | - | - |
| 6.3 | O.TK.6305 | - | - | - |
| 7.8 | O.TK.7805 | - | - | - |

TW= C-type thermocouple
TK= K-type thermocouple

## Table 3  Time chart of the KATS control system for test KATS-7

| Test KATS-7 | |
|---|---|
| Event | Time (s) |
| Ignition of thermite powder<br>Start video cameras | 0 |
| Start of melt release out of crucible<br>Start transient recorder<br>Trigger flashlight | 21.0 |
| Start of moving chute | 29.0 |
| Chute on end position | 31.5 |

## Tab. 4 Pouring rates for iron and oxide melts in test KATS-7

### Iron melt

| Time (s) | Flow rate (l/s) |
|----------|-----------------|
| 0.0      | 3.00            |
| 1.0      | 2.98            |
| 2.0      | 2.97            |
| 3.0      | 2.96            |
| 4.0      | 2.97            |
| 5.0      | 2.98            |
| 6.0      | 3.00            |
| 6.20     | 3.00            |
| 6.21     | 0.0             |

### Oxide melt

| Time (s) | Flow rate (l/s) |
|----------|-----------------|
| 0.0      | 3.27            |
| 1.0      | 3.32            |
| 2.0      | 3.38            |
| 3.0      | 3.42            |
| 4.0      | 3.47            |
| 5.0      | 3.49            |
| 6.0      | 3.50            |
| 7.0      | 3.47            |
| 8.0      | 3.39            |
| 9.0      | 3.24            |
| 10.0     | 2.98            |
| 11.0     | 2.55            |
| 12.0     | 1.85            |
| 13.0     | 0.71            |
| 13.3     | 0.23            |
| 13.4     | 0.0             |

## Table 5  Arrival times and velocities of iron melt at axial and vertical thermocouple locations in test KATS-7

| Axial position of thermocouples (m) | Melt arrival times (s) Melt velocity (m/s) Vertical positions of thermocouples | | | |
|---|---|---|---|---|
| | 5 mm | 15 mm | 25 mm | 35 mm |
| 0.3 | 1.98 | (no thermocouple) | (no thermocouple) | (no thermocouple) |
| | 0.47 m/s | - | - | - |
| 1.8 | 5.14 | 5.85 | *) | - |
| | 0.39 m/s | - | - | - |
| 3.3 | 8.93 | (no thermocouple) | *) | (no thermocouple) |
| | 0.36 m/s | - | - | - |
| 4.8 | 13.06 | 13.3 | *) | (no thermocouple) |
| | 0.27 m/s | - | - | - |
| 6.3 | 18.66 | (no thermocouple) | (no thermocouple) | (no thermocouple) |

The velocities are melt front velocities between two consecutive axial thermocouple positions at identical vertical locations.
*) Evaluation of melt arrival times not possible.

## Table 6 Arrival times and velocities of oxide melt at axial and vertical thermocouple locations in test KATS-7

| Axial position of thermocouples (m) | Melt arrival times (s) Melt velocity (m/s) Vertical positions of thermocouples | | | |
|---|---|---|---|---|
| | 5 mm | 15 mm | 25 mm | 35 mm |
| 0.3 | 2.85 | (no thermocouple) | (no thermocouple) | (no thermocouple) |
| | 0.45 m/s | - | - | - |
| 1.8 | 6.18 | 6.6 | 7.0 | - |
| | 0.30 m/s | 0.29 m/s | - | - |
| 3.3 | 11.18 | 11.7 | *) | (no thermocouple) |
| | 0.25 m/s | 0.27 m/s | - | - |
| 4.8 | 17.2 | 17.3 | (no thermocouple) | (no thermocouple) |

The velocities are melt front velocities between two consecutive axial thermocouple positions at identical vertical locations.
*) Evaluation of melt arrival times not possible.
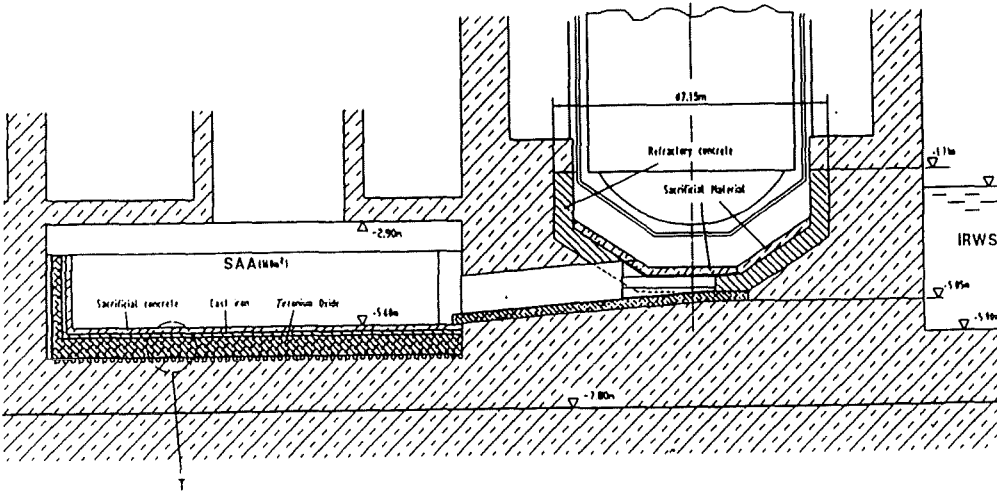
# Fig.1 Improved Reference Concept of the EPR Core-melt Retention System
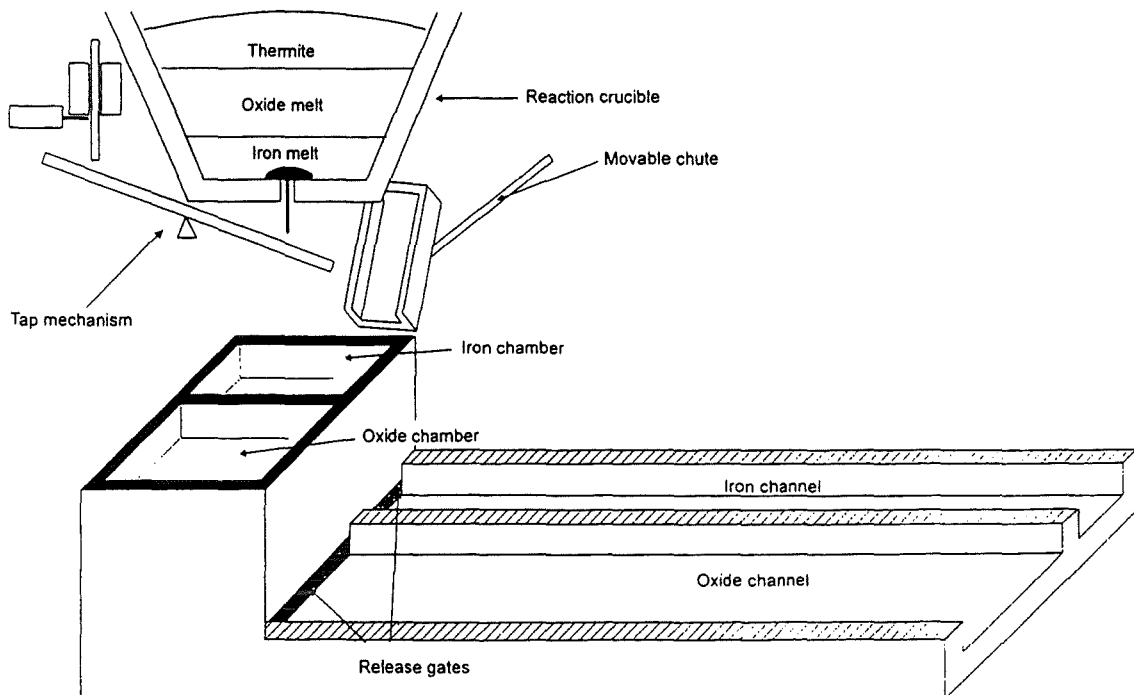


# Fig.2 Schematics of the KATS Facility
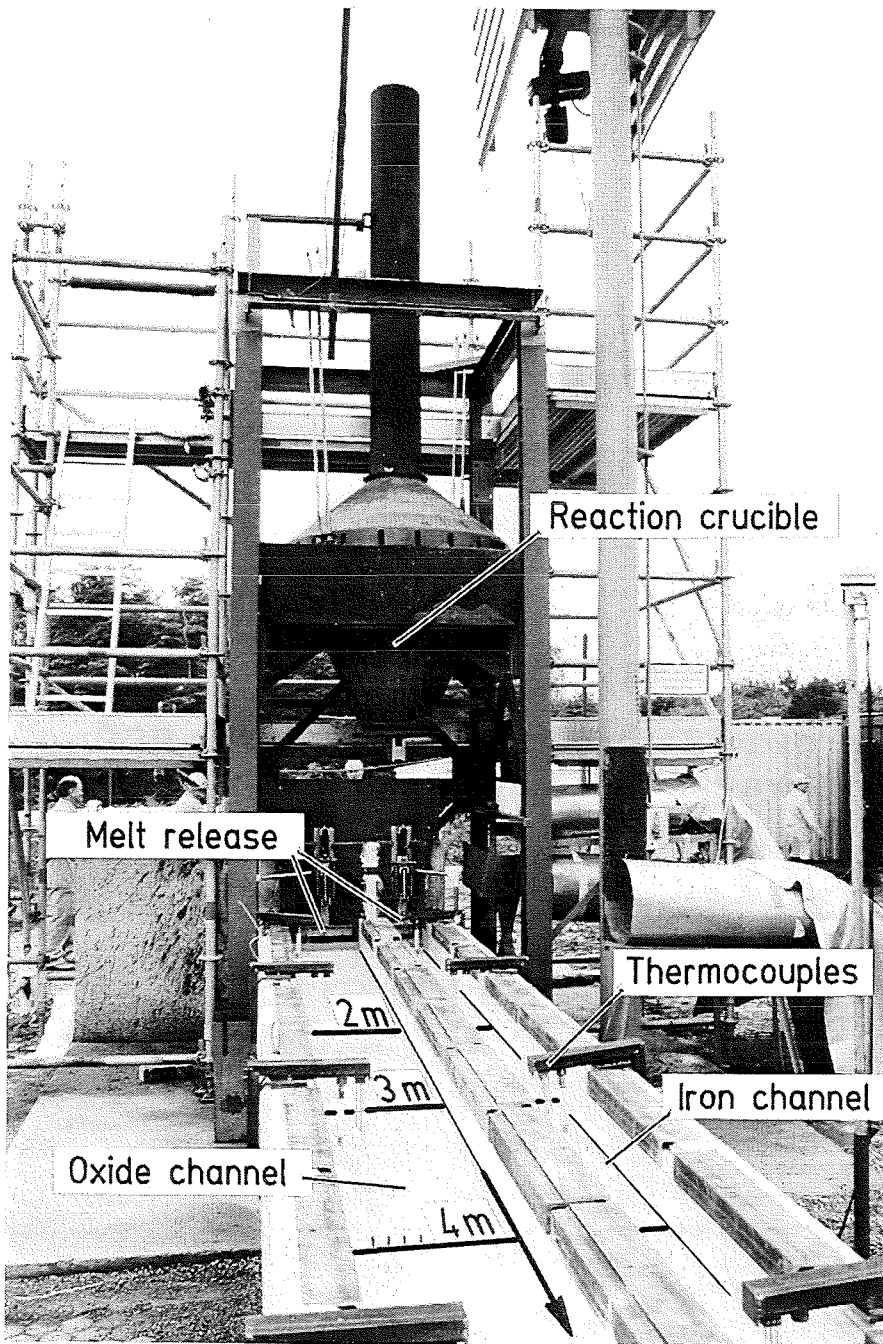
Fig. 3 Photo of the KATS Facility
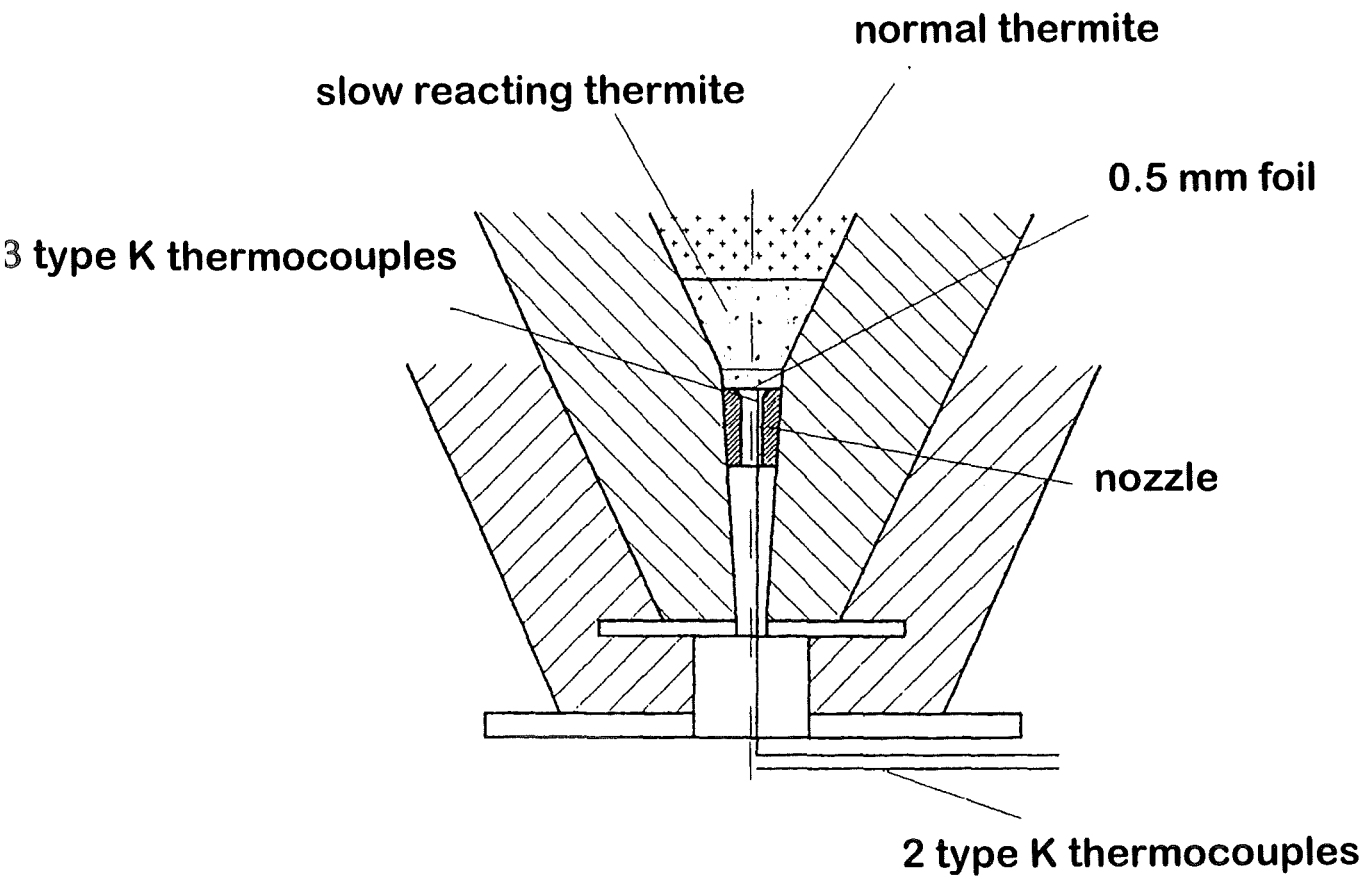
**Fig. 4 Bottom of reaction crucible with nozzle**
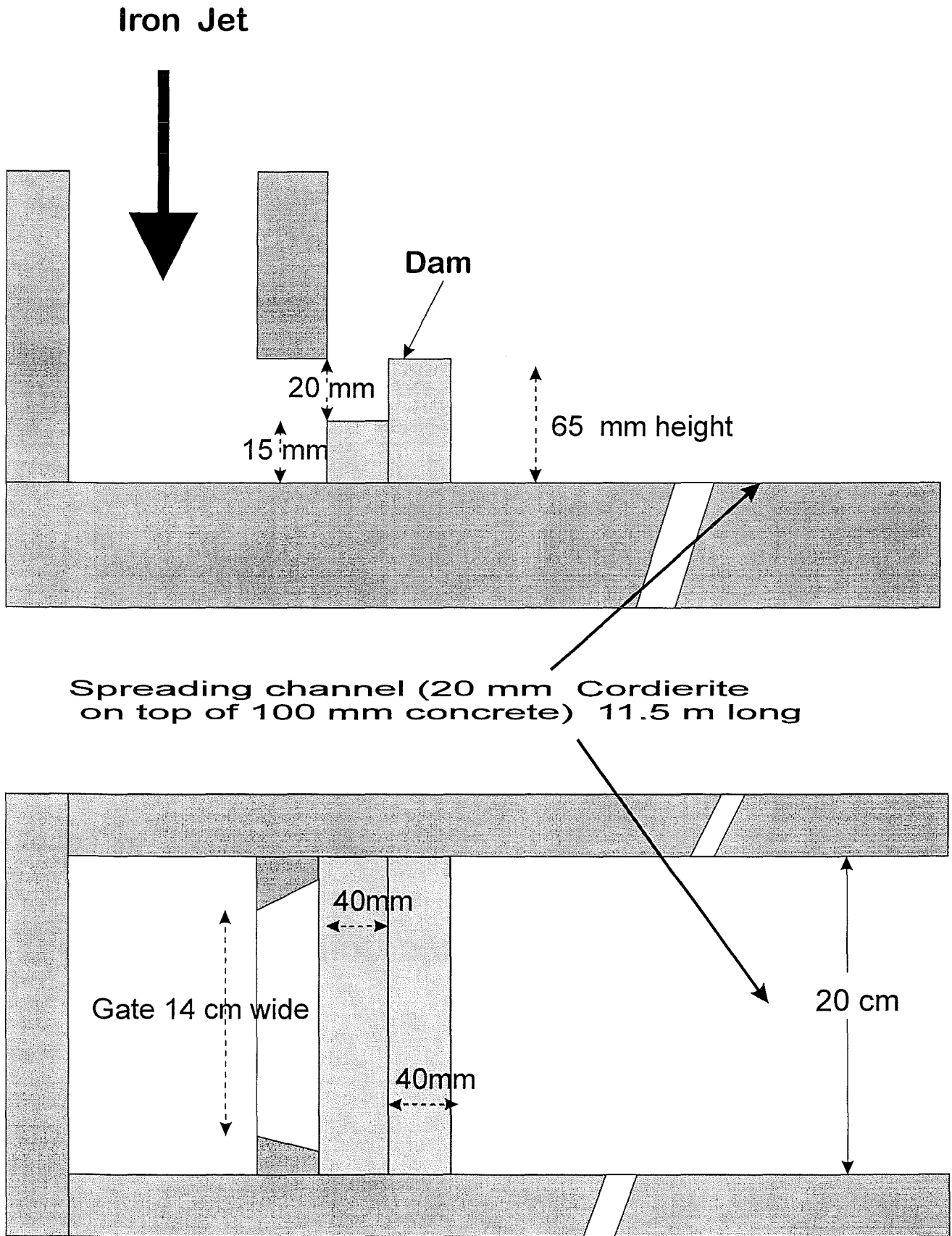
Fig. 5 Layout and dimensions for the spreading of iron melt in test KATS-7
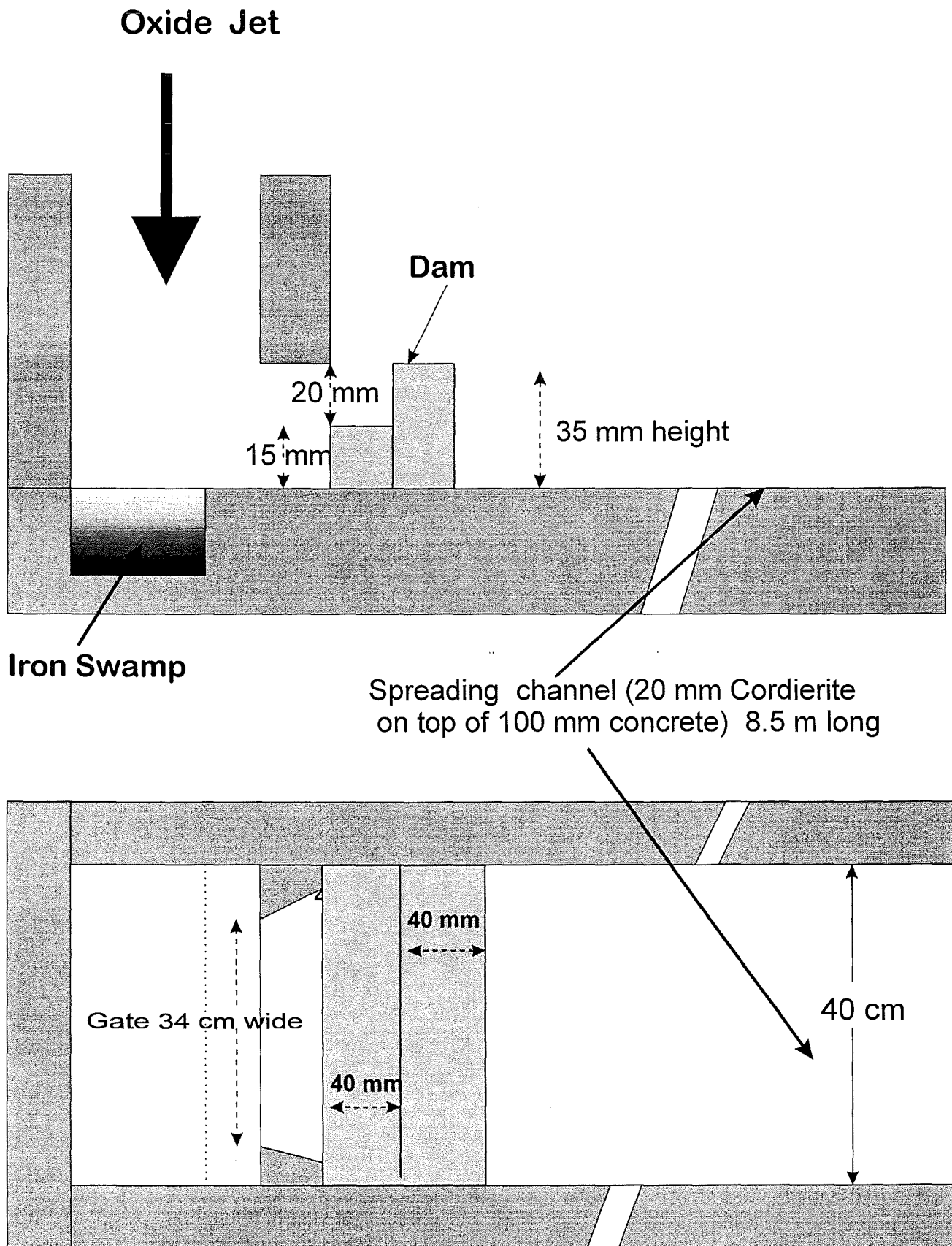
Fig. 6 Layout and dimensions for the spreading of oxide melt in test KATS-7

TW - thermocouples to measure temperature
TK - thermocouples to detect the arrival of the melt



| E.TK.1845 | | | |
| E.TK.1825 | E.TK.3325 | E.TK.4845 | |
| E.TK.1815 | | E.TK.4825 | |
| E.TK.0305 | E.TK.1805 | E.TK.3305 | E.TK.4805 | E.TK.6305 | E.TK.7805 | E.TK.9305 | E.TK.10805 |
| E.TW.0305 | E.TW.1805 | | E.TW.4805 | | | | |

iron

2,5m     5,5m     8,5m     11,5m

oxide

flow direction ⟹

O.TW.0005
O.TK.0305

O.TW.1805
O.TK.1805
O.TK.1815
O.TK.1825
O.TK.1835

O.TK.3305
O.TK.3315
O.TK.3325

O.TW.4805
O.TK.4805
O.TK.4815

O.TK.6305

O.TK.7805

0,3m    1,8m    3,3m    4,8m    6,3m    7,8m    9,3m    10,8m
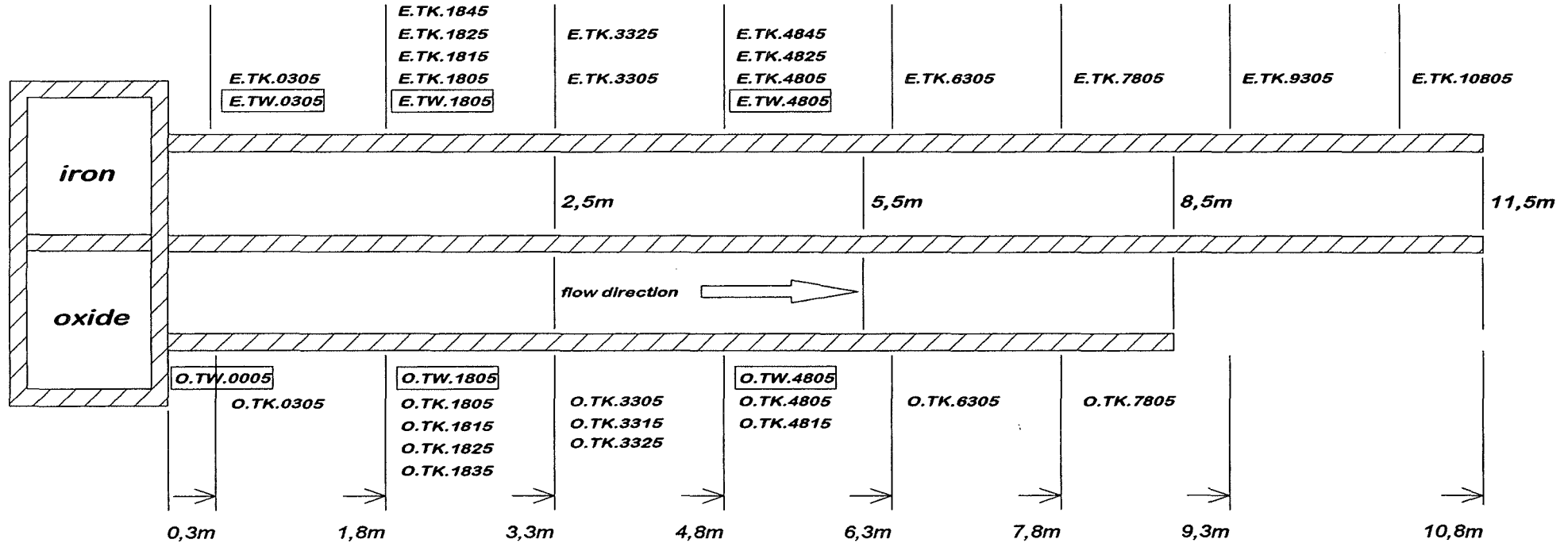
explanation :

TK = thermocouples type K
TW = thermocouples type W-Re
E = iron - channel
O = oxide - channel

1825 = position 1,8 m , height 25 mm

Fig. 7    *Locations of thermocouples in test   KATS - 7*
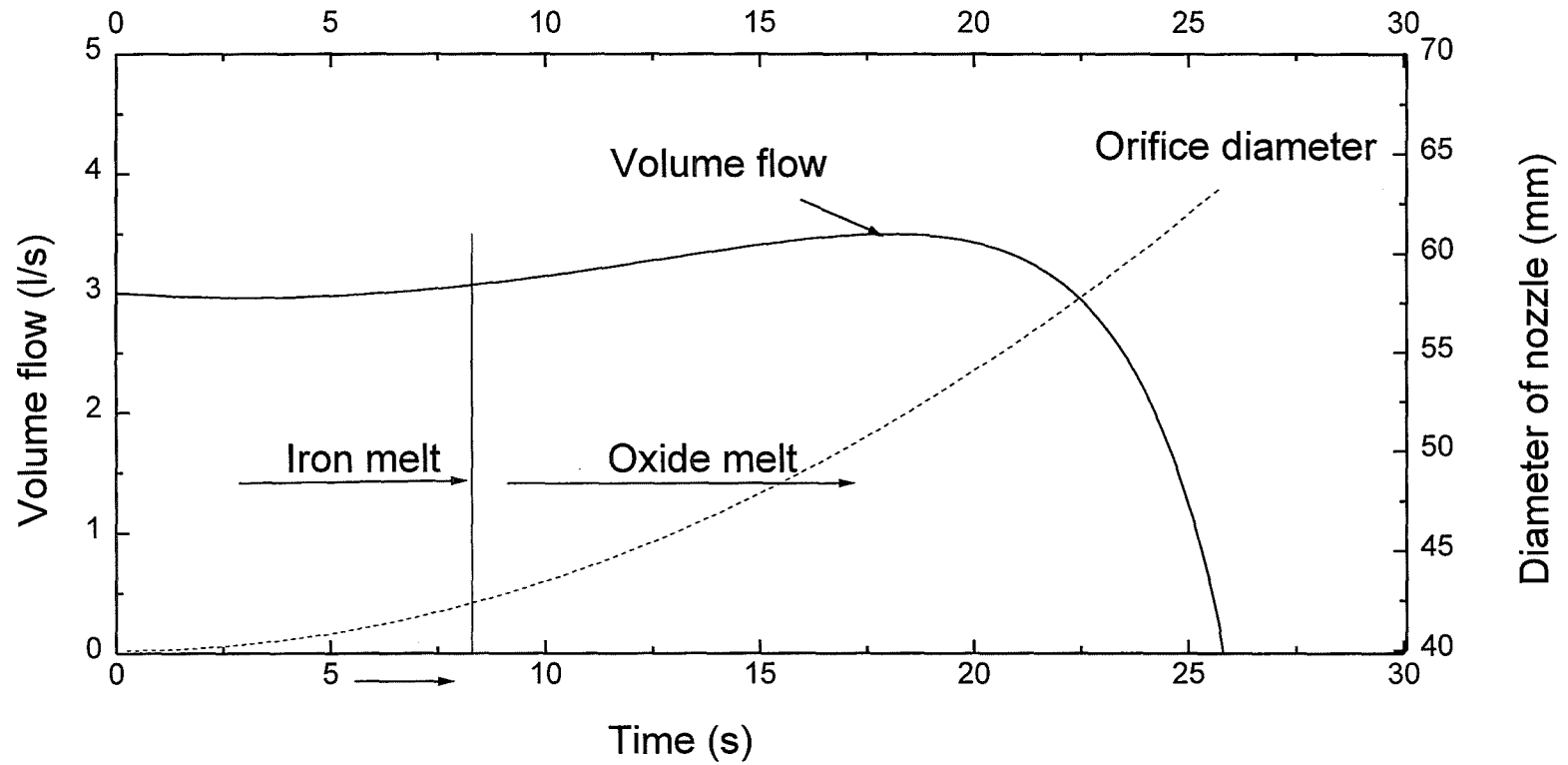
Fig.8 Transient volume flows for iron and oxidic melts from the thermite reaction crucible in test KATS-7 calculated for the increasing orifice diameter of the nozzle

23

Entrance

0.0m       1.0m       2.0m       3.0m       4.0m       5.0m

0.5   1.0 2.0   2.5    3.0   3.5    4.0   4.5 5.0    5.5   6.0   6.5    7.0 7.5   8.0   8.5   9.0    9.5   10.0 10.5 11 11.5   12.   12.5 13.   13.5

24

⟶ Flow direction ⟶

5.0m       6.0m       7.0m       8.0m

13.5    14.    15. 16.    17.    18. 19. 20. 21. 22.     25.   27.5     32.5 s   time after start of pouring (s)
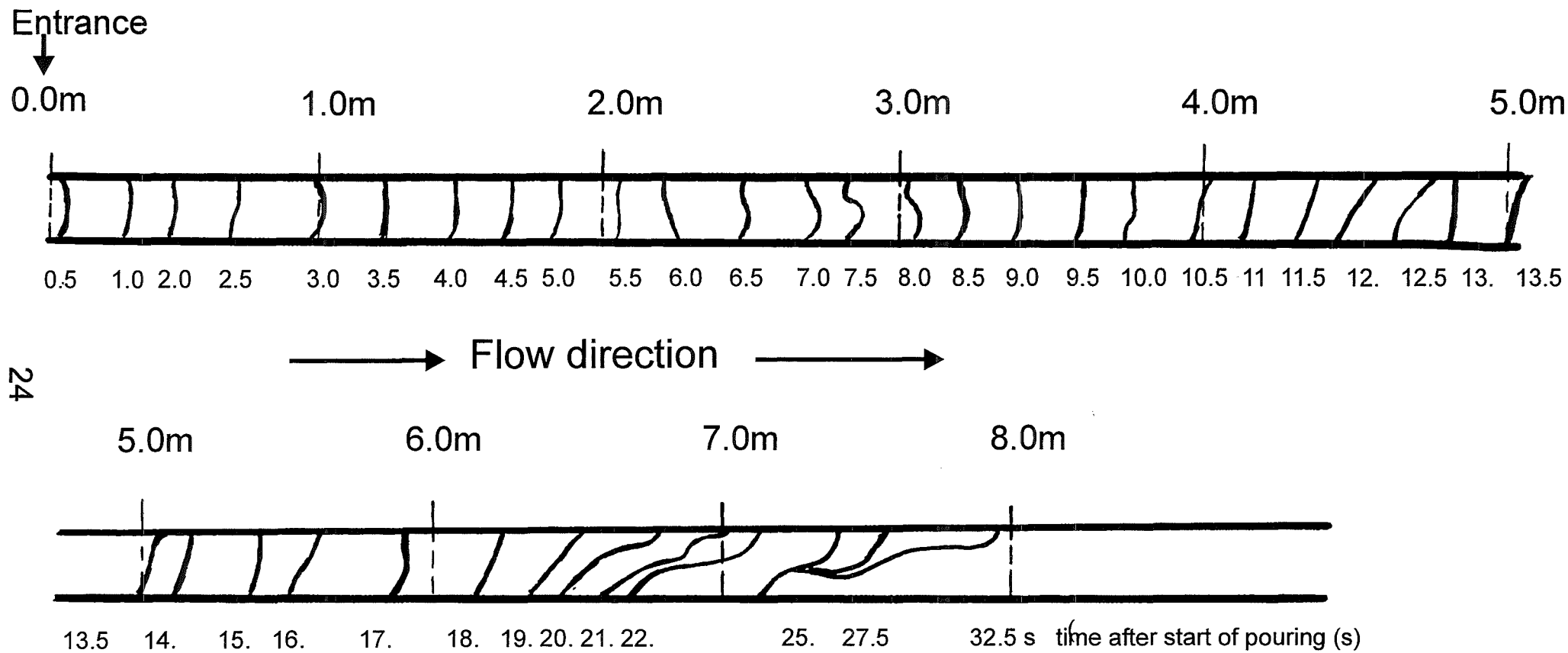
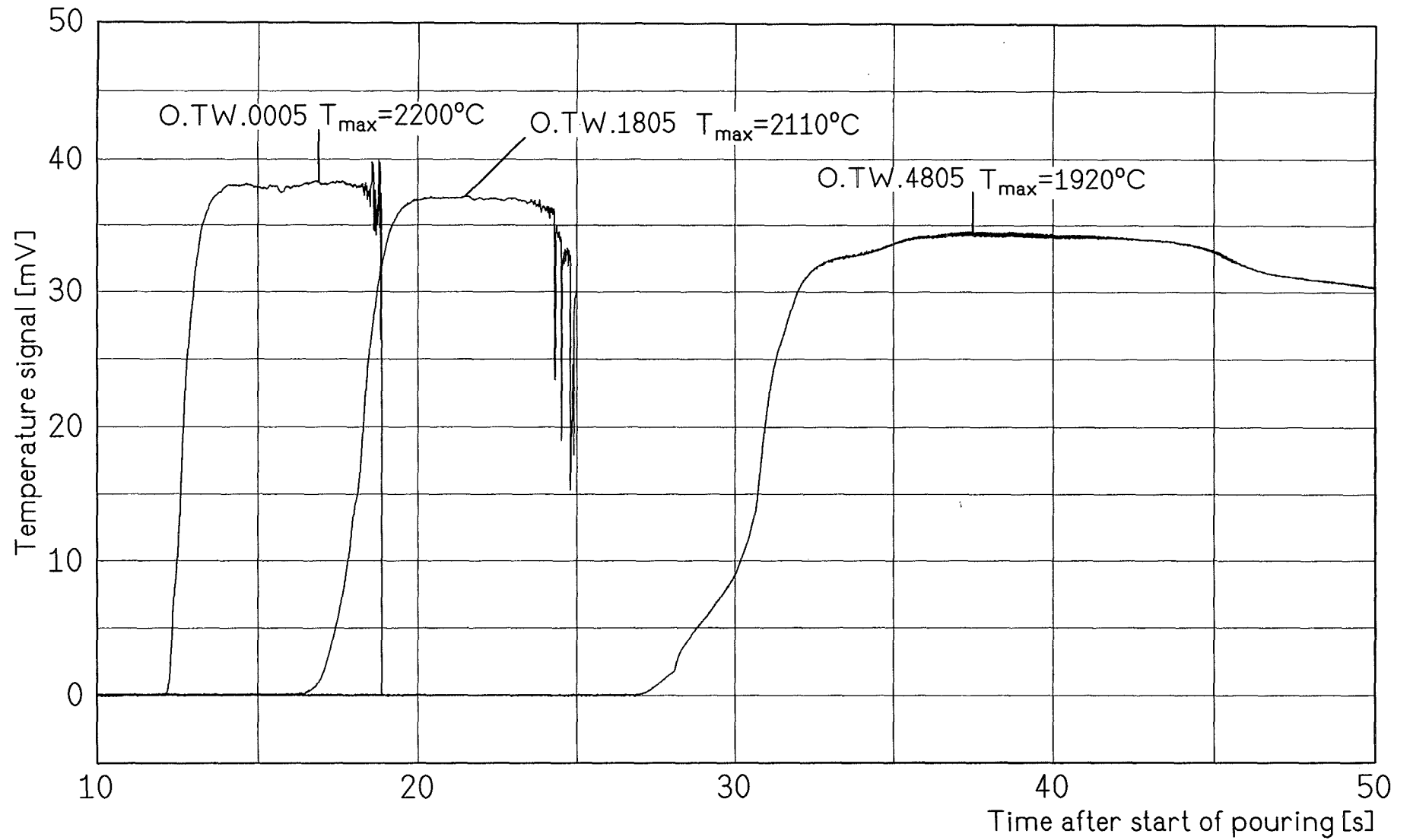**Fig. 9 Transient spreading of iron melt into dry channel for test KATS-7**
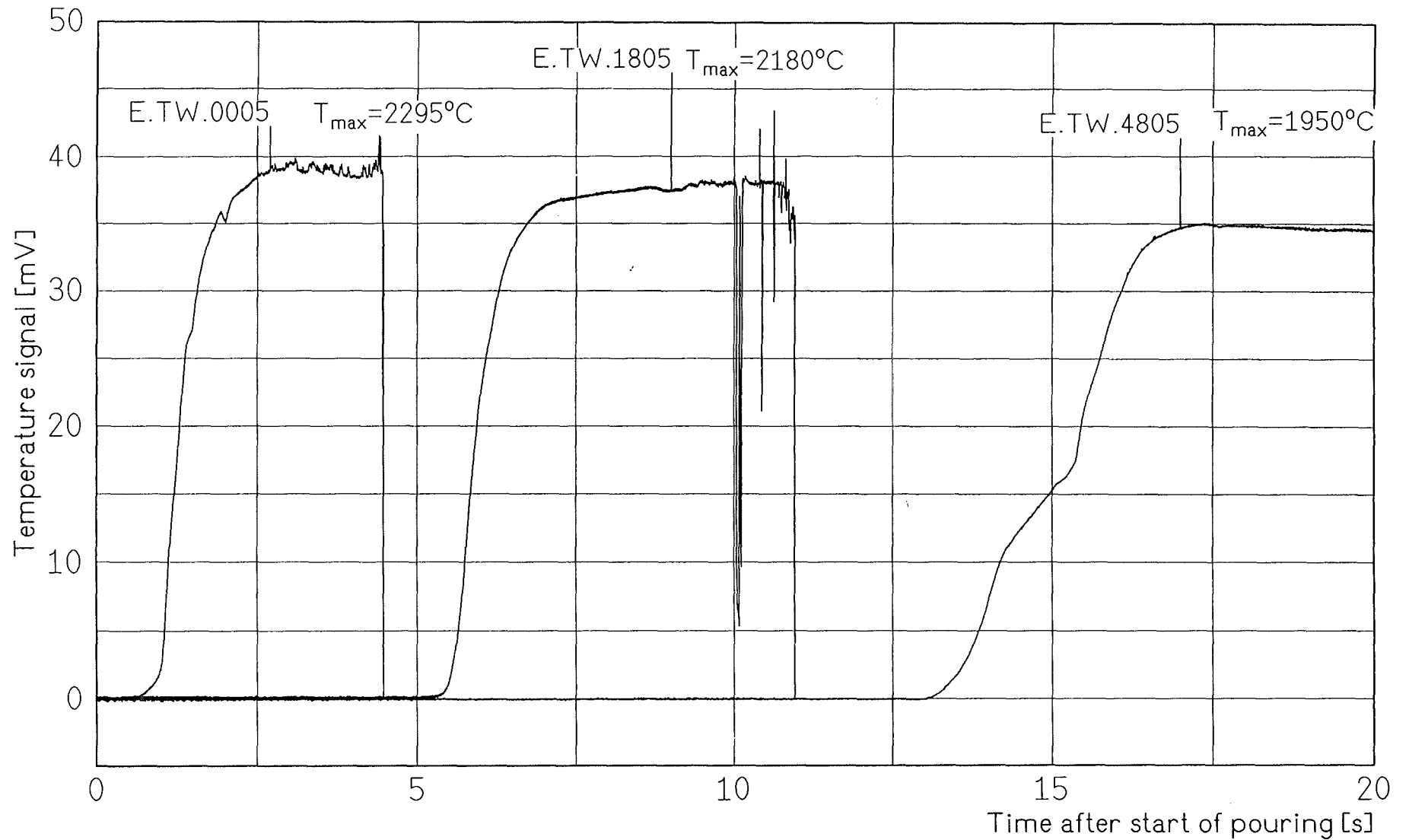
Fig. 10  Test KATS-7  Temperature of the iron melt at positions 0.05 / 1.8 / 4.8 m
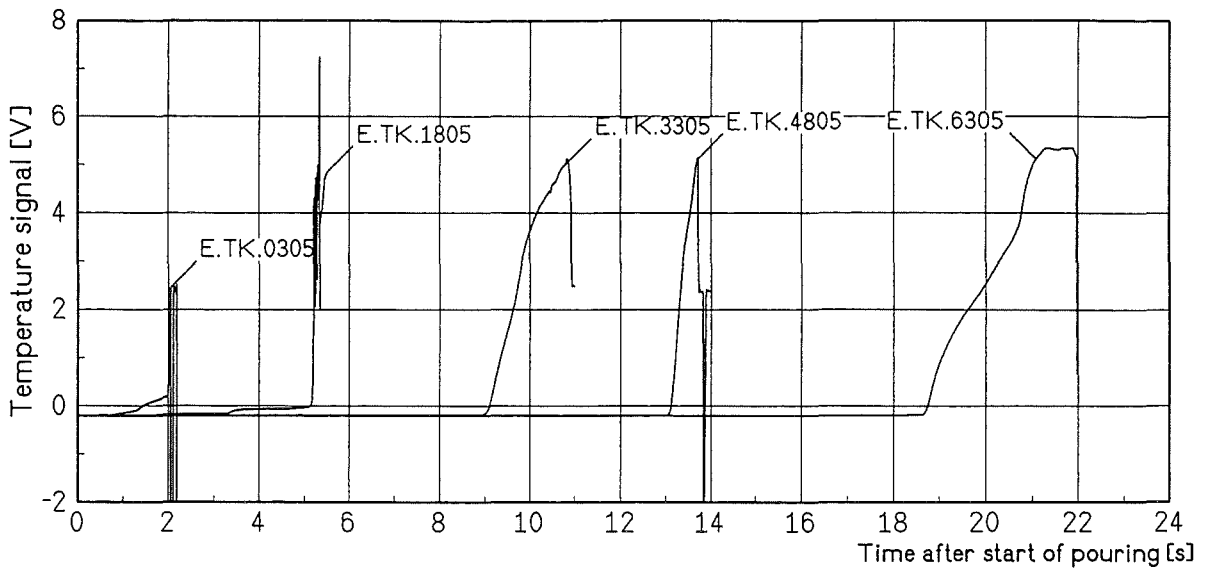
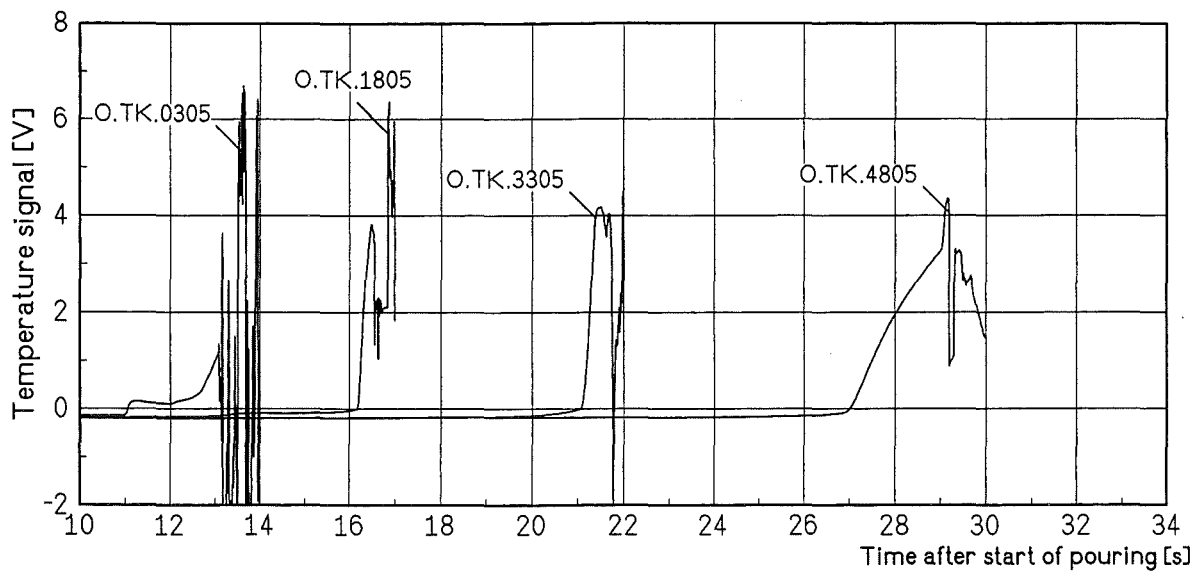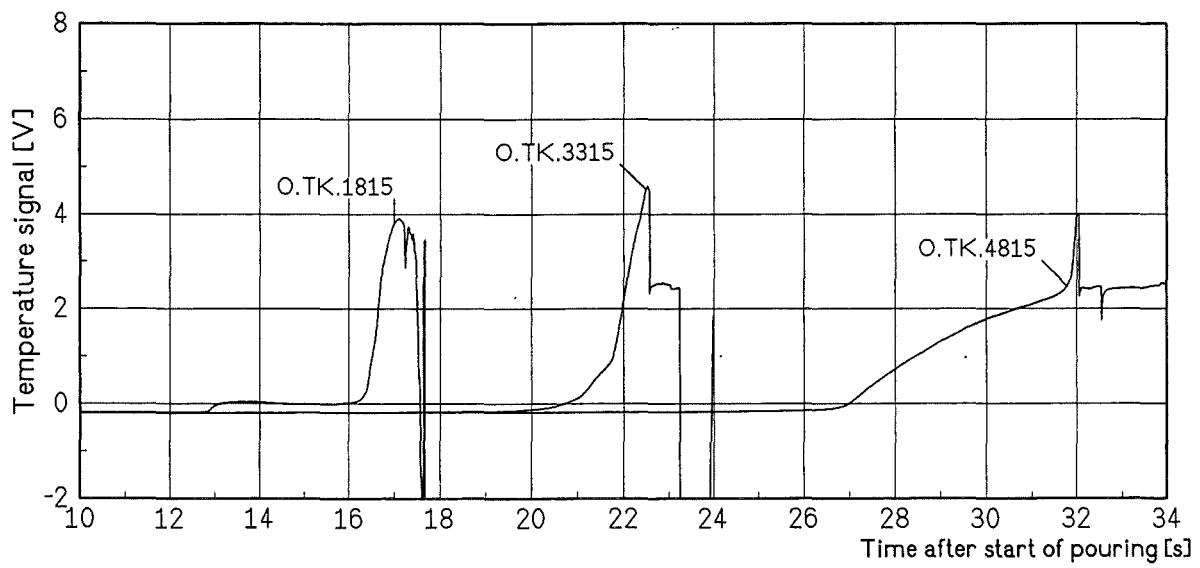Fig. 11   Test KATS-7   Detection of the iron melt at 5mm height
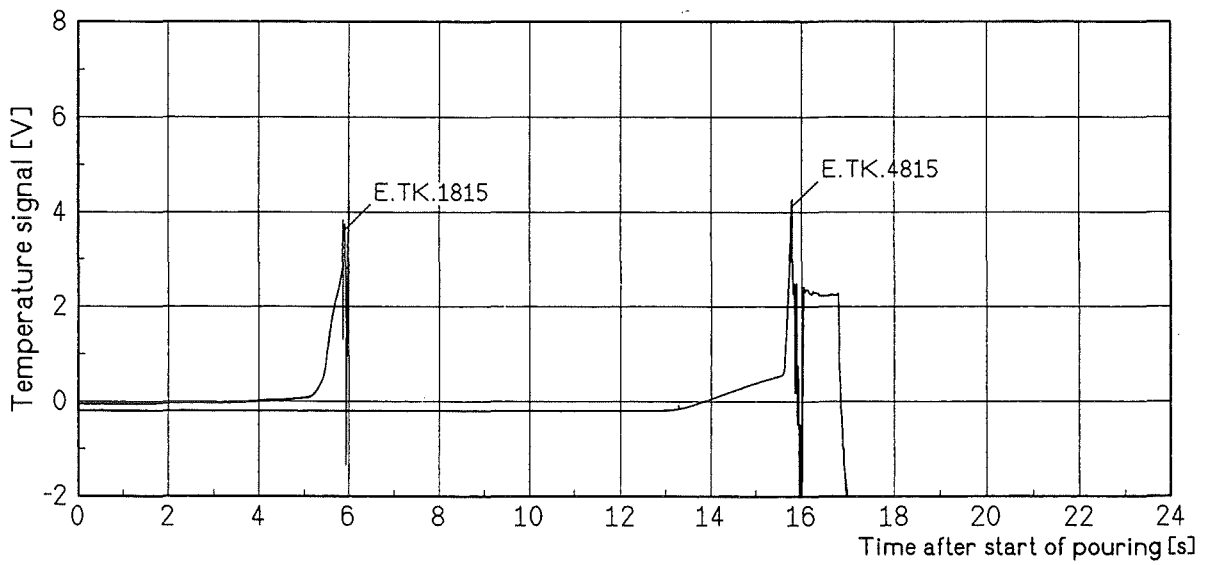


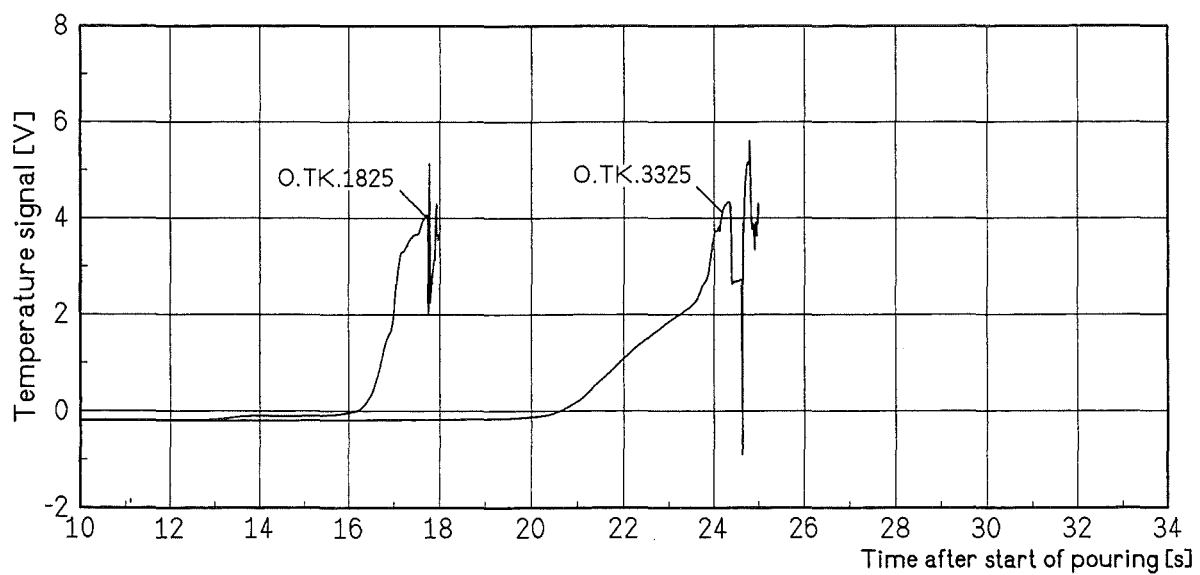Fig. 12   Test KATS-7   Detection of the iron melt at 15mm height
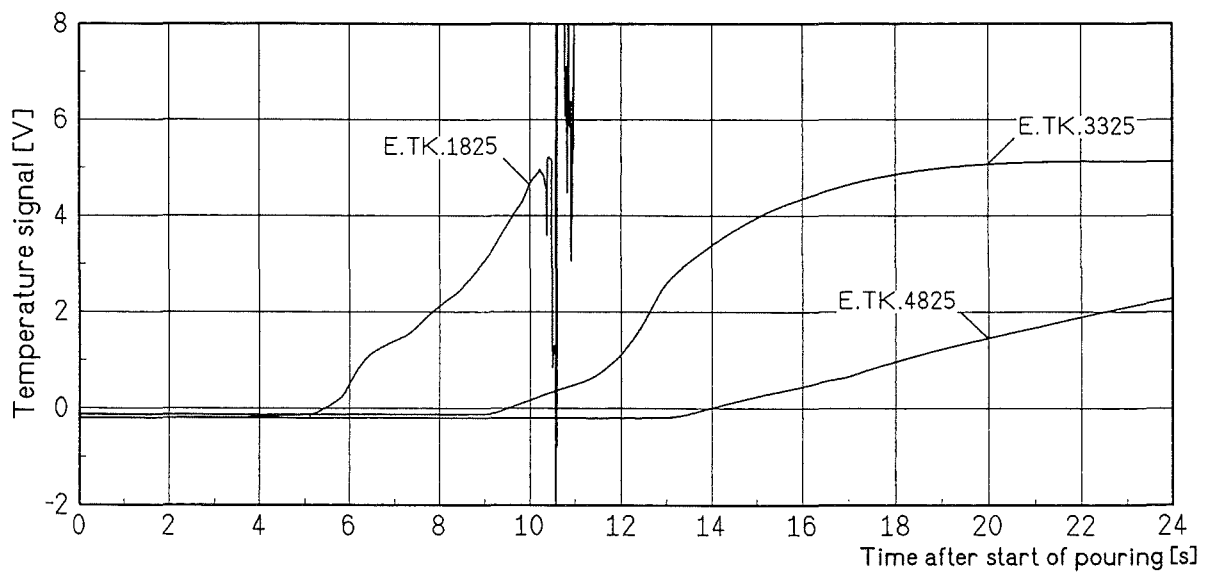


Fig. 13   Test KATS-7   Detection of the iron melt at 25mm height
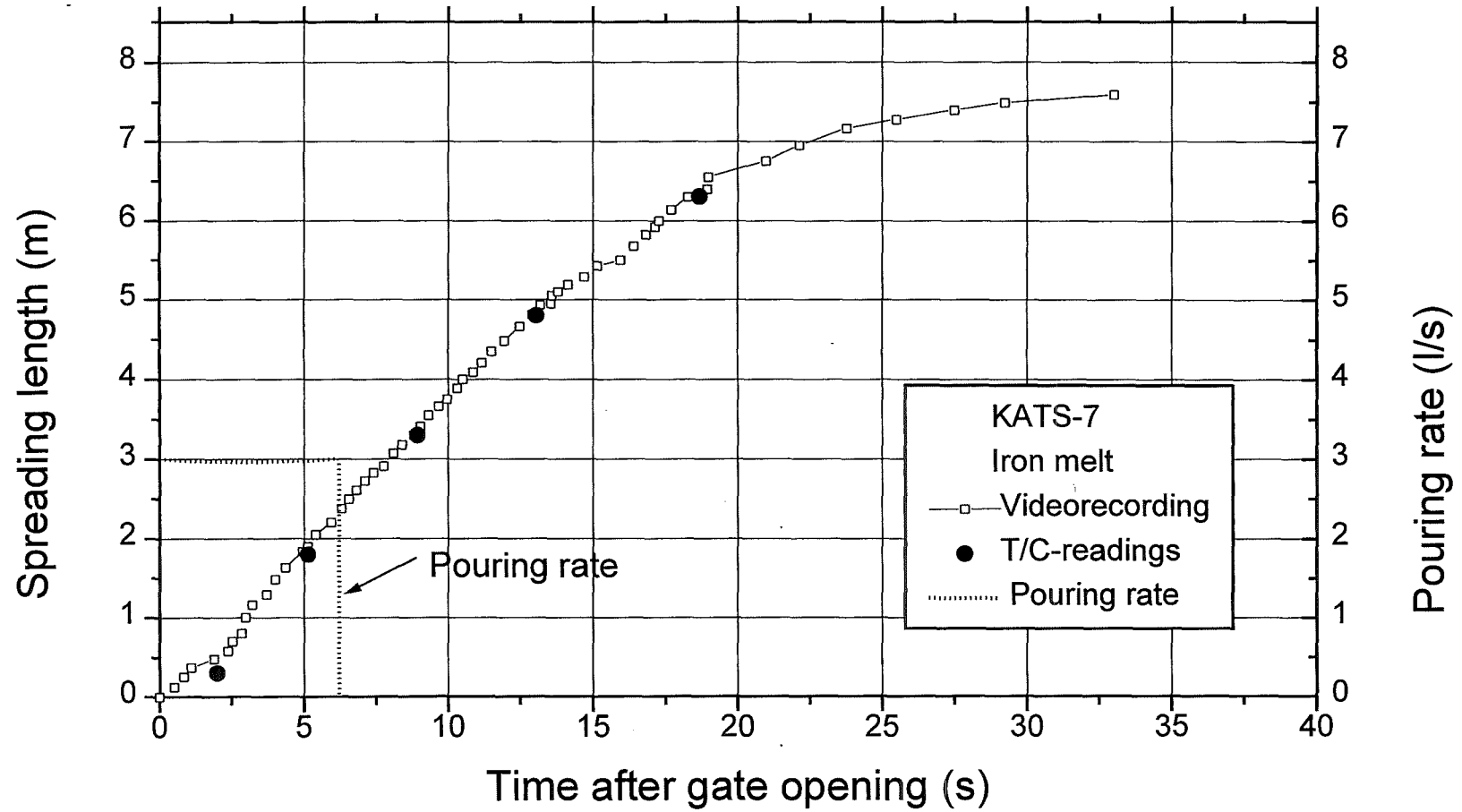
Fig. 14 Transient leading edge propagation of the iron melt

27

Flow Direction ⟶
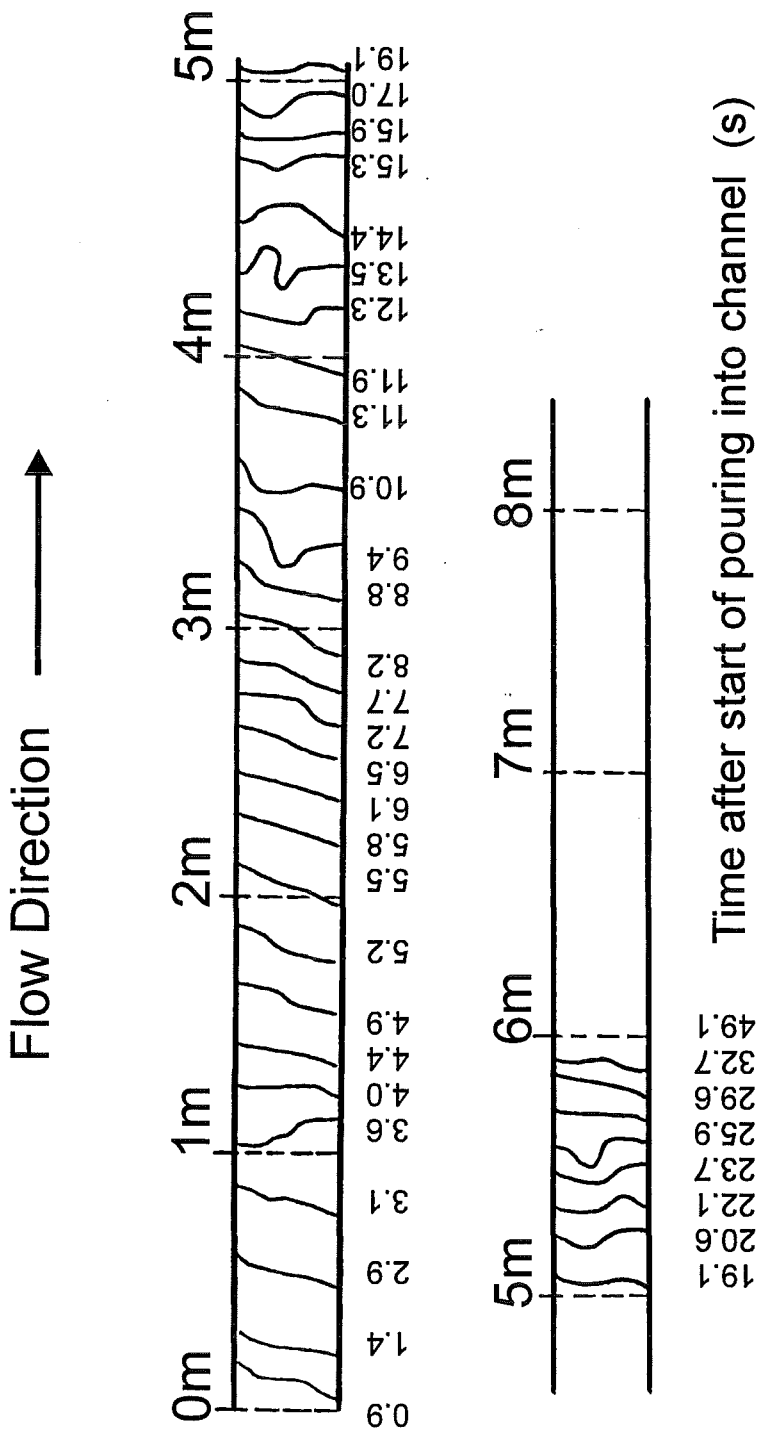


Fig. 15  Transient spreading of oxidic melt into dry channel in test KATS-7

Fig. 16 Test KATS-7 Temperature of the oxide melt at positions 0.05 / 1.8 / 4.8 m

The chart is labeled with the following:

- O.TW.0005 $T_{max}$=2200°C
- O.TW.1805 $T_{max}$=2110°C
- O.TW.4805 $T_{max}$=1920°C

Y-axis: Temperature signal [mV], ranging from 0 to 50

X-axis: Time after start of pouring [s], ranging from 10 to 50

29

Fig. 17 Test KATS-7 Detection of the oxide melt at 5mm height



Fig. 18 Test KATS-7 Detection of the oxide melt at 15mm height



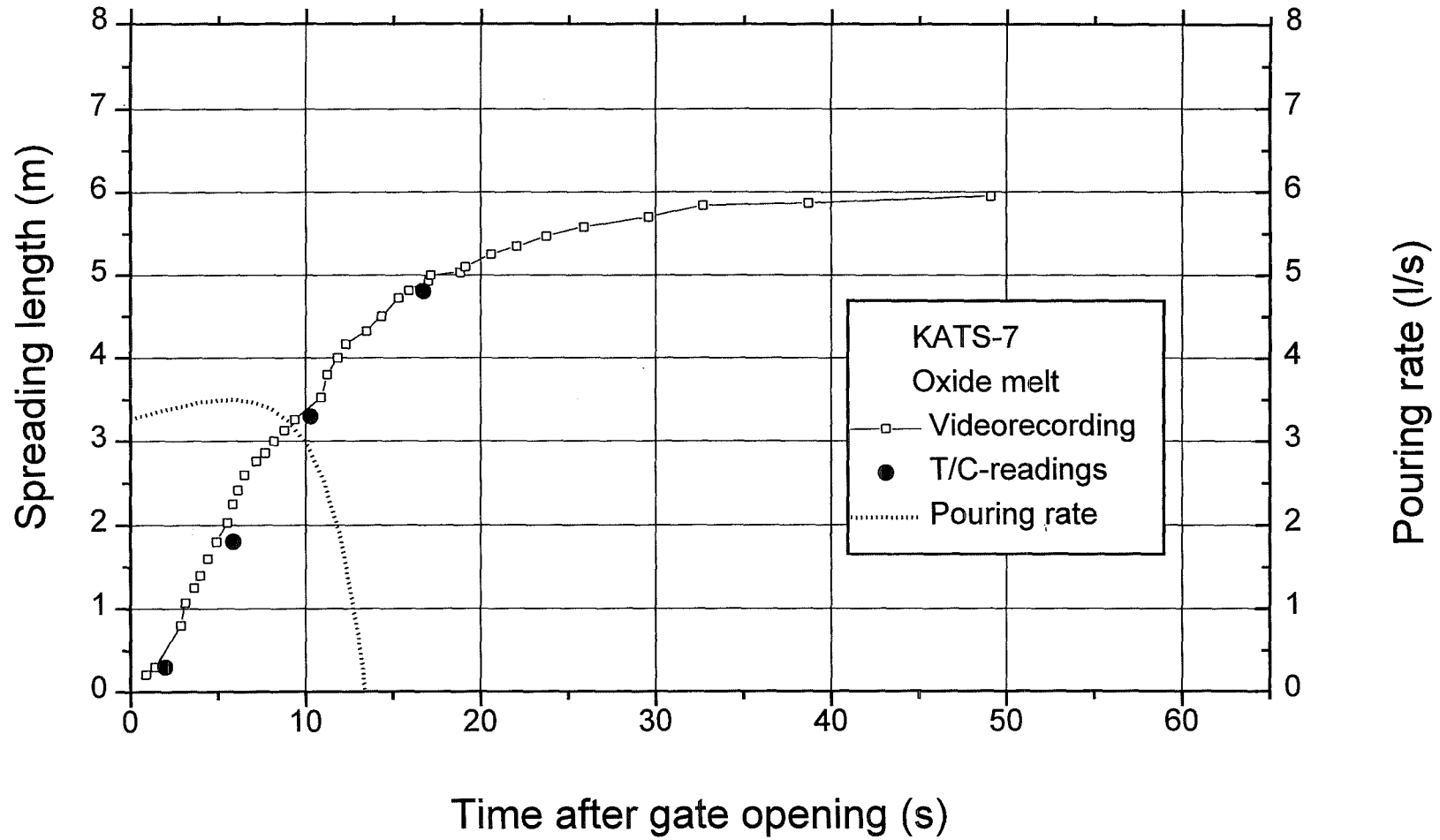Fig. 19 Test KATS-7 Detection of the oxide melt at 25mm height

30

Fig. 20  Transient leading edge propagation of oxide melt

# Appendix A: Material Properties

The KATS tests are performed to verify spreading codes like CORFLOW. Therefore the knowledge of material properties is of tremendous importance. The data for iron melts are rather well known /A-1/, as to oxidic melts, especially mixtures of oxides as used in KATS-7, there is only a limited base of property data available. Some programmes are underway to determine such data. So far, however, one has to use best estimate data which originating from data of similar mixtures, some few experimental data and theoretical modelling.

Some material property data are presented here which are recommended to use in CORFLOW calculations, as long as now newer experimental data are available. More information in detail is given in ref. /A-1/.

To evaluate material data like viscosity, specific enthalpy, specific heat and specific density, the results of GEMINI calculations /A-2/ are necessary. GEMINI defines the solidus and liquidus temperatures of a composite oxide including the fraction of solidified particles in the fluid. Stedman's correlation /A-3/ has been applied to evaluate the viscosity within the solid-liquidus range, above liquidus experimental data from Elyutin et. al. /A-4/ have been applied. Specific enthalpies in the fully solidus and liquidus ranges have been evaluated using the enthalpies of the individual oxides by weighing their molar fractions in the composite oxide. Within the solidus-liquidus range results of the Gemini calculations have also been used. In the same way as the specific enthalpy, the specific density has been evaluated, except that the weighing of individual oxides is done by their fractions of weight rather than molar weight. In figs A-1 through A-4 the results of this evaluation are shown.

References:

/A-1/ G. Fieg, "Recommended material property data to analyze KATS experiments with the CORFLOW code", to be published

/A-2/ M. Steinbrück, private communication

/A-3/ J.M. Seiler, J. Ganzhorn, "Viscosities of Corium-Concrete Mixtures, 14th European Conf. On Thermophysical Properties", INSA, Lyon, France, September 16-19, 1996

/A-4/ V.P. Elyutin et. al., "Viscosity of alumina", Russian Journal of Physical Chemistry, 43(3), 1969

# Table A-1 Material properties of oxidic KATS melt

| viscosity | | diff. enthalpy *) | | spec. density | |
|---|---|---|---|---|---|
| Temp ($^0$C) | cP | Temp ($^0$C) | J/kgK | Temp ($^0$C) | kg/m3 |
| 1777 | ∞ | 27 | 768 | 1500 | 3821 |
| 1794 | 6006 | 107 | 913 | 1577 | 3811 |
| 1817 | 1600 | 307 | 1065 | 1604 | 3721 |
| 1838 | 756 | 507 | 1131 | 1677 | 3605 |
| 1876 | 306 | 807 | 1193 | 1755 | 3470 |
| 1900 | 174 | 1207 | 1251 | 1817 | 3325 |
| 1917 | 117 | 1577 | 1333 | 1900 | 3065 |
| 1925 | 100 | 1587 | 4789 | 1925 | 2917 |
| 2000 | 81 | 1597 | 4537 | 2000 | 2845 |
| 2100 | 59 | 1607 | 4302 | 2200 | 2652 |
| 2200 | 43 | 1617 | 4085 | 2400 | 2459 |
| 2300. | 32 | 1657 | 3400 | 2500 | 2363 |
| 2350 | 28 | 1737 | 2895 | | |
| | | 1757 | 2951 | | |
| | | 1827 | 3717 | | |
| | | 1927 | 6362 | | |
| | | 1937 | 1389 | | |
| | | 2007 | 1391 | | |
| | | 2607 | 1400 | | |

*) The phase change of ironoxide between 1300 and 1400 $^0$C has been omitted here, because it is not important in terms of high temperature melt spreading
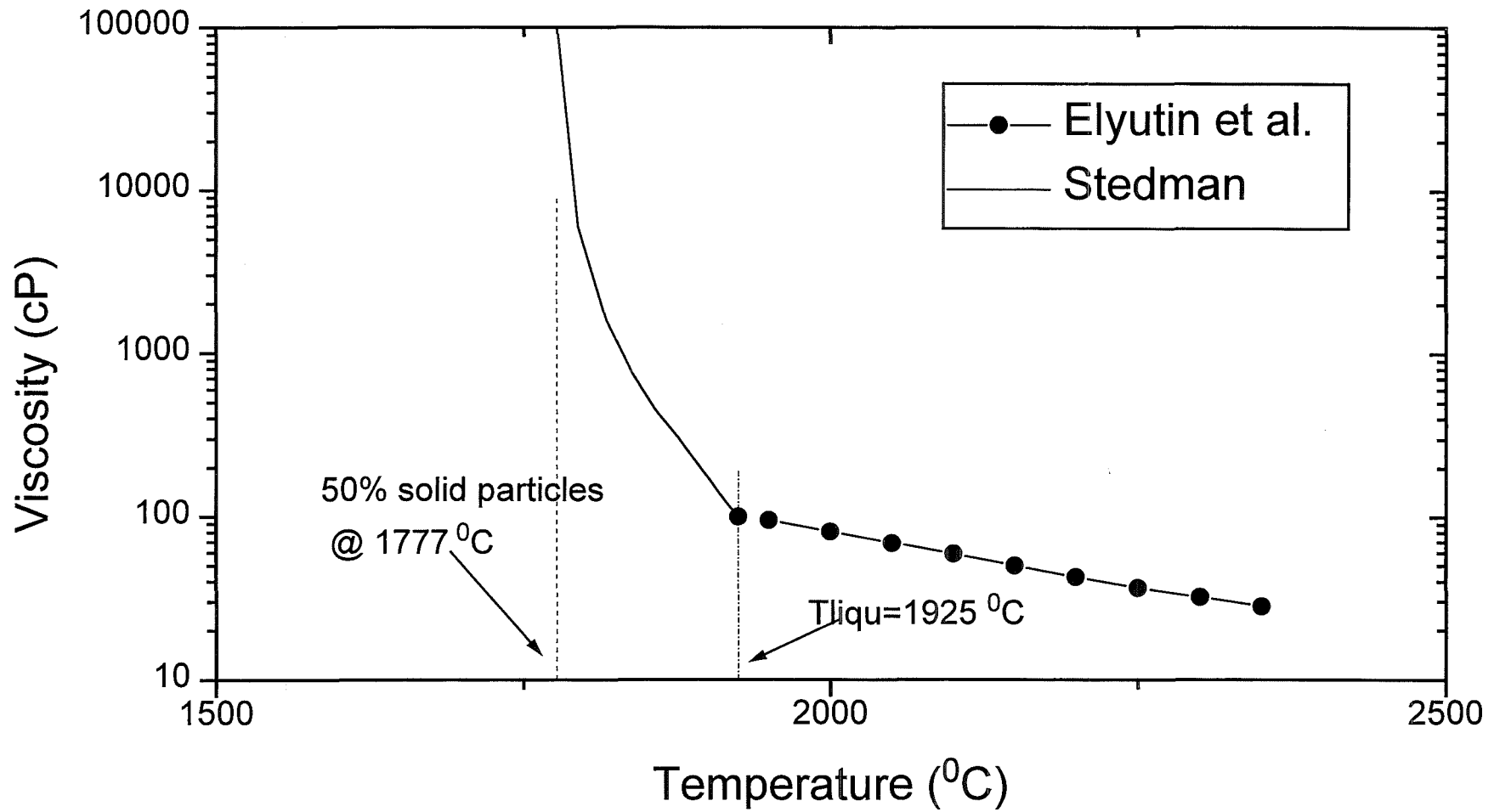
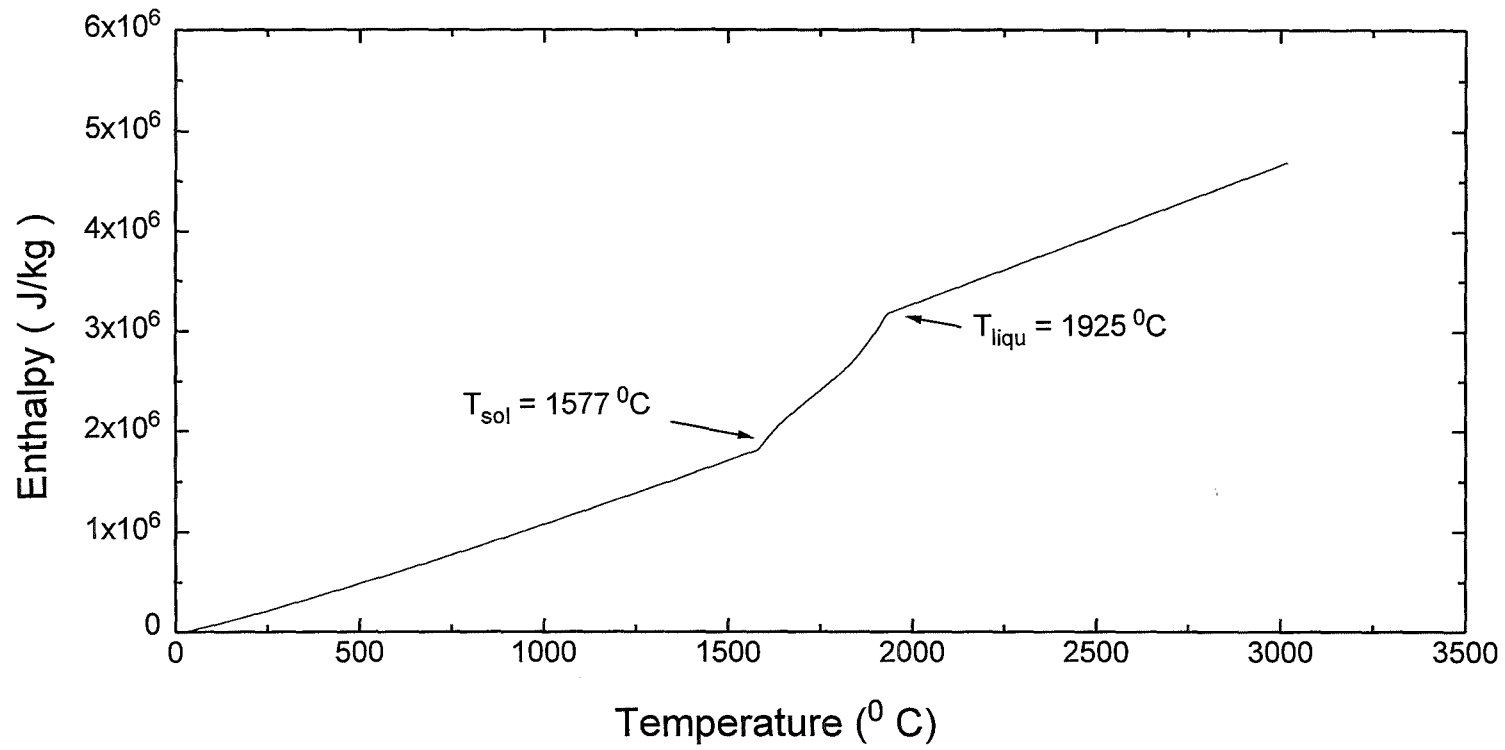Fig. A-1 Temperature dependant viscosity of the oxidic KATS melt
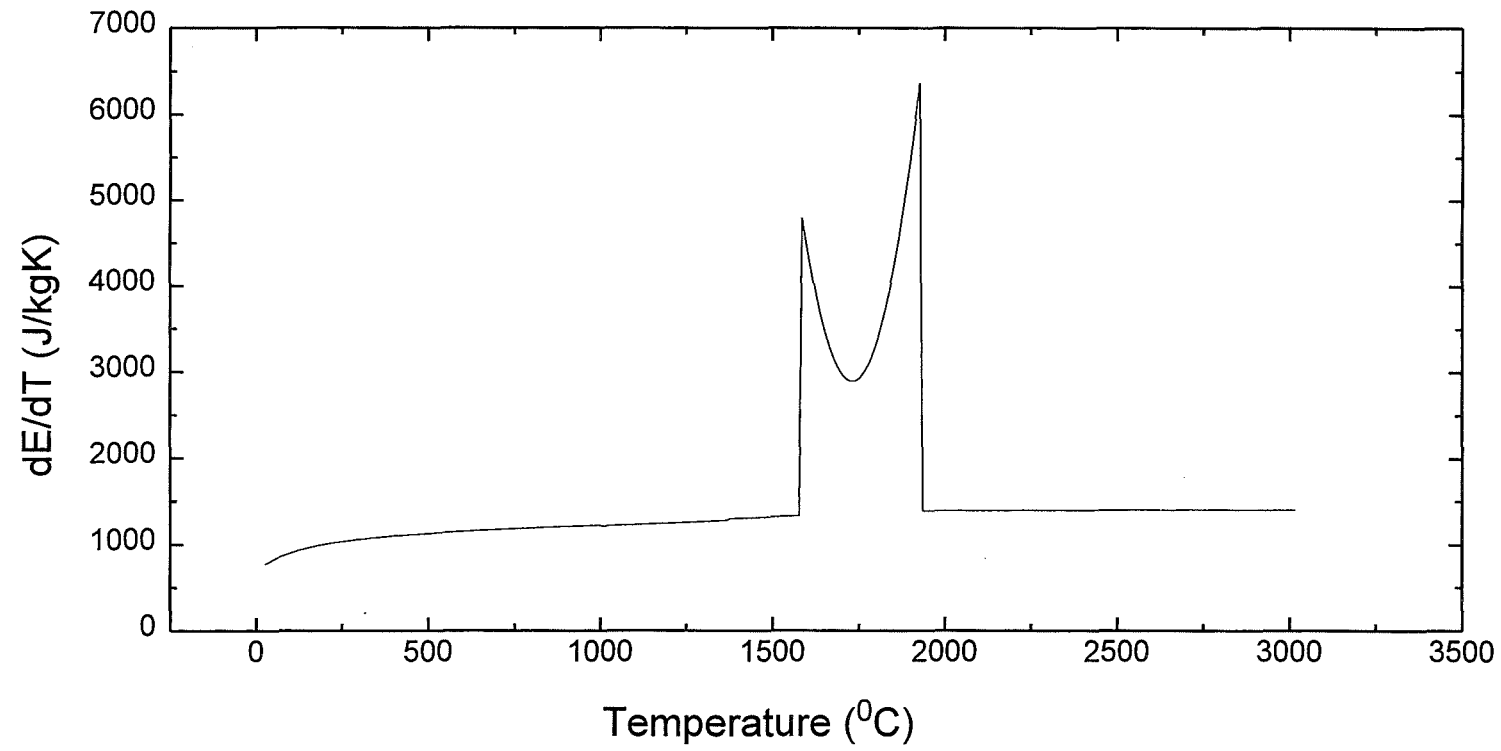
Fig. A-2 Specific enthalpy of oxidic KATS melt
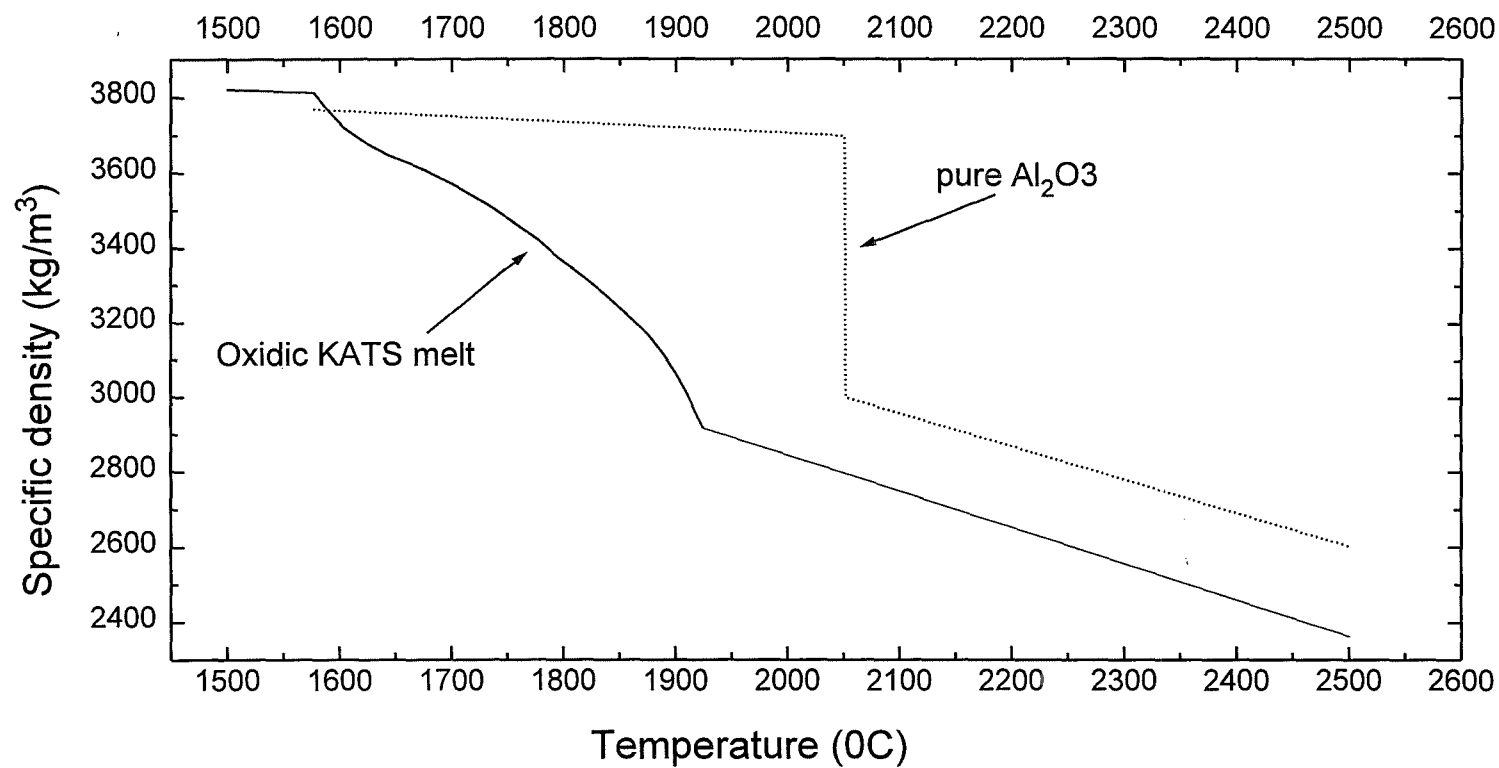
Fig. A-3 Differential enthalpy dE/dT of the oxidic KATS melt

Fig. A-3 Temperature dependant specific density of oxidic KATS melt